Chapter 4

Case study: Cooperative deployment

Introduction

The cooperative deployment of two satellite in formation will be studied in the frame of the indirect optimization methods. After a brief introduction about the Simbol-X transfer orbit, the optimal thrust direction and magnitude and the switching function will be introduced. The optimal control theory will be applied first on a single satellite deployment, then on satellite formation deployment. Approximate control law and errors in thrust will be also considered.

4.1 Mission in HEO: Simbol-X

In section 1.2 the mission used as case study was introduced. The indirect method optimization is applied to the deployment phase, first considering only a single satellite, then considering the formation deployment. The two satellites are injected by the launcher into an initial elliptic orbit and then they perform an orbit transfer to move on the operational orbit.

The initial and final orbits are highly elliptic and their orbital parameters are shown in table (4.1). It is possible to see that the transfer orbit is mainly a perigee raising, so the engine burns will be placed mainly at the apogee.

The HE orbits have a low perigee, so perturbations due to asphericity of the Earth have to been taken in account, especially at the beginning of the transfer. The high apogee needs inclusion of the luni-solar perturbation, while solar radiation pressure is important in the formation keeping and can be important if the mass to surface ratio is different between the two satellites, in particular in long missions.

The missions requires two spacecrafts, the mirror and the receiver and they will

Table 4.1: Initial and final orbit characteristics.

	a, km	e	i, deg	Ω, deg	ω, deg	ν	r_p,km	r_a,km
initial	98922	0.931985	5.2	90.0	270.0	0.0	6728	191116
final	106247	0.798788	-	-	-	180.0	21378	191116

be indicated as SAT1 and SAT2. The properties of the two satellites are presented in Table (4.2).

Table 4.2: Satellites Properties.

	SAT1	SAT2
Launch mass [kg]	960	1250
Propellant mass [kg]	150	200
Mean surface $[m^2]$	5.7	4.2
Initial S/m	$5.94 \cdot 10^{-3} m^2/kg$	$3.36 \cdot 10^{-3} m^2/kg$
T [N]	8N	8N
Isp [s]	220	220

The two satellites have different mass and different surface, but they have the same thruster which produces $T = 8N$. Other thrust levels have been also used in this thesis. The thruster exploits hydrazine as propellant (while fine formation thrusters use cold gas). Having two different masses, the two satellites have also different acceleration and so SAT1 is lighter and more agile with respect to SAT2. These features will influence the mission deployment strategy.

The two satellites are injected by the launcher directly at the perigee of orbit A , but, in order to have proper separation, SAT1 has an initial ΔV of 0.50 m/s. So the SAT1 initial orbit is slighter different from the SAT2 orbit, with an higher apogee and longer period. Mission prescribes that the two satellites have to arrive at the same final orbit B. Only semimajor axis and eccentricity are prescribed, leaving the other orbital parameters free. But the final orbit has to be the same for both satellites. For operational reason no burns are permitted in the first revolution of the two satellites, so the first phase is pure coasting and only at the following apogee perigee passage the satellites can fire their engines.

The two satellites, in order to observe the universe, need a relative distance in the order of 20 meters, so at the end of the deployment phase the two satellites should

have a relative distance of 10 kms in order to start proximity maneuvers, further details are given in section 1.2. The deployment phase is considered terminated when, at apogee, the same orbit and the final relative distance of 10 km are reached. At the last apogee of the deployment the proximity manoeuvres will start, and so no burns are permitted at the last apogee. No time-transfer and departure date constraints are imposed, so different multi-revolution missions are analyzed.

In chapter 3 the dynamic models used in this thesis have been introduced, giving a general frame for trajectories optimization. The starting point is the shape of the initial and final orbit. They are both HEOs, but the initial reference orbit has a low perigee, so the influence of the asphericity of the Earth is relevant. From the first simulations was also clear that J2 perturbations was very important in the first revolution and also in the overall strategy of the burns times. This aspect will be deeper analyzed in sec. 5.1.1, but it is important to note here that J2 effects on semimajor axis are null in average in a complete revolution, but if the two satellites are injected at the perigee, the results is an instant drop of the semimajor axis that will change the optimal strategy. A 8x8 model of Earth's potential is introduced. Drag is neglected, because the time passed in the lower atmosphere is considered negligible.

The high apogee makes Moon and Sun perturbations very important. Satellites perigee shows significant variations even considering only the ballistic flight.

Lunar perturbation brakes or accelerates the spacecraft when it is at the apogee, changing its semi-major axis, perigee and orbital period. The period changes the next apogee passage (when compared with the 2 body solution) and so it is difficult to forecast the position of the Moon and its influence at the next revolution. The effect of these perturbations on the switching structures for the optimal fuel save deployment is hard to predict.

The perturbation of the Moon in the first revolution of the spacecraft, that is ballistic, can lower the perigee and makes the spacecraft plunging in the atmosphere. The impossibility of controlling the spacecraft orbit in the first phase of the mission makes important the analysis of moon influence and the choice of the departure date.

Solar radiation pressure is a very little perturbation, if compared with the other ones, but it has a strong impact when avoidance collision for the formation flight is considered because the satellites have different S/m and the period in which formation keeping is active is longer. Even if in this specific problem seems to be negligible (but this results is found a posteriori) it is worth to take into account this perturbation for different possible m/S ratio for the two spacecraft.

4.2 Optimal values of the control

In section 2.4 the indirect method was introduced and eq. (2.33) is the algebraic expression for the optimal control. The dynamical model of the problem has been introduced in chapter (3) and the only control present is the thrust vector $\boldsymbol{T}$. This means that the control can be represented by the three components of the thrust T_u, T_v, T_w or using the magnitude T and the thrust angles γ_T and ψ_T, as defined in eq. (3.37).

For the sake of clearness here the Hamiltonian of eq. (3.28) is re-written in a compact form, emphasizing the dependence on thrust and where H' collects all the terms that do not contain the control

$$H = \boldsymbol{\lambda}^T \boldsymbol{x} = H' + \boldsymbol{\lambda_V}^T \boldsymbol{T}/m - \lambda_m(T/c) \tag{4.1}$$

$\boldsymbol{\lambda_V}$ is the adjoint vector to velocity and in literature is called primer vector [67]; its magnitude is λ_V. The expression of the primer vector is:

$$\boldsymbol{\lambda_V} = \lambda_u \boldsymbol{\imath} + \lambda_v \boldsymbol{\jmath} + \lambda_w \boldsymbol{k} \tag{4.2}$$

The projection of the thrust vector direction on the primer vector is indicated as

$$\Lambda_T = \lambda_u T_u/T + \lambda_v T_v/T + \lambda_w T_w/T \tag{4.3}$$

The Hamiltonian can be written as

$$H = \boldsymbol{\lambda}^T \boldsymbol{x} = H' + T(\Lambda_T/m - \lambda_m/c) = H' + T \cdot S_F \tag{4.4}$$

$S_F = (\Lambda_T/m - \lambda_m/c)$ is the Switching function and it is called in this way because its sign determines if the thruster is switched ON or OFF. From optimal control theory, the optimal thrust magnitude should be derived from $\partial H/\partial T = 0$, but the Hamiltonian is linear with the thrust magnitude. However, PMP states that the optimal control is the value that maximizes the Hamiltonian. So if the switching function is positive, the optimal value of thrust is T_{max}, otherwise is null. In equation is

$$T = \begin{cases} T_{max} & \text{for} \quad S_F > 0 \\ 0 & \text{for} \quad S_F < 0 \end{cases} \tag{4.5}$$

The control is bang-bang.

The optimal thrust elevation angle γ_T and thrust heading angle ψ_T are found by posing $\partial H/\partial \gamma_T = 0$ and $\partial H/\partial \psi_T = 0$. These equations provide

$$\sin\gamma_T = \lambda_u/\lambda_V \tag{4.6}$$

$$\cos\gamma_T \cos\psi_T = \lambda_v/\lambda_V \tag{4.7}$$

$$\cos\gamma_T \sin\psi_T = \lambda_w/\lambda_V \tag{4.8}$$

These are the cosine director of the primer vector. In other words the optimal direction of the thrust is parallel to the primer vector. If the optimal strategy is adopted $\Lambda_T = \lambda_V$.

4.3 Single satellite optimal control

Most of the considerations and the procedure developed for the optimization of the single satellite optimization are valid even for the formation flight. For the single satellite transfer is considered a satellite with physical property identical to SAT1 (i.e. $m_0 = 960kg$), but the initial orbit is equal at the reference one (so the initial $\Delta V = 0$). This satellite will be named SAT0.

The statement of the problem is described in section (4.1). From the statement the mathematical formulation of the boundary conditions has to be derived. The dynamical equations, the differential equations for adjoint variables, optimality and transversality conditions define the problem.

The dynamical equations and differential equations are defined in chapter (3)

At the initial point $j = 0$ all state variables are assigned. In the optimal procedure the initial time t_0 is considered to be given. A parametric analysis to evaluate the influence of the departure date on the mission has been performed. At the final point $j = f$ apogee radius r_A and orbit semilatus rectum $p = a(1 - e^2)$ are given. The final point is the apogee. The conditions of the state variables at the terminal point are:

$$r_f - r_A = 0 \tag{4.9}$$
$$u_f = 0 \tag{4.10}$$
$$v_f^2 + w_f^2 - \mu p / r_A^2 = 0 \tag{4.11}$$

The performance index to be maximized is the final mass $\phi = m_f$. The optimality conditions (2.35-2.36), eliminating the adjoint constants, are:

$$\lambda_{\vartheta f} = 0 \tag{4.12}$$
$$\lambda_{\varphi f} = 0 \tag{4.13}$$
$$\lambda_{vf} w_f - \lambda_{wf} v_f = 0 \tag{4.14}$$
$$\lambda_{mf} = 1 \tag{4.15}$$

As said before the final time is free, so the transversality condition (2.38) gives Hamiltonian null at the end.

$$H_f = 0 \tag{4.16}$$

Application of equations 2.35 and 2.36 at every switch point gives Hamiltonian continuity. State and adjoints variables are also continuous and so the switching function has to be null at the switch points (Points where engines turns OFF-ON or vice-versa)

$$S_{Fj} = 0 \qquad j = 1, \ldots, f-1 \tag{4.17}$$

The numerical problem consists of 14 differential equations represented by (3.10-3.16) and (3.29-3.35). The state variables initial values are given, but the initial values of the adjoint state variables are unknown. The lengths of the coast and burn arcs are also unknown; an equal number of boundary conditions, given by Eqs. (4.9)-(4.17) completes the MPBVP.

The problem is homogeneous in the adjoint variables and Eq. (4.15) can be replaced by assigning the initial value $\lambda_{m0} = 1$ in order to reduce the number of unknowns. All these parameters are included in the parameters vector $\boldsymbol{p}$.

The indirect method needs a good initial guess to have an optimal solution. For this reason the research team started with a simplified model of the problem, without perturbations, for having a tentative guess for the more complex problem. The first attempt have tried to solve the two body problem with the shortest mission possible, that was 2.5 revolutions. The orbit transfer is mainly a perigee raising and a little apogee decrease. The proto-mission was a long burn arc at apogee followed by a very short one at perigee (see [68]). In thesis the burn arc at perigee is indicated with P, while the one at apogee is indicated with A. The first ballistic revolution is omitted. The proto mission is described with A-P. If the the transfer time is increased the number of revolutions can be 3.5, 4.5 and so on. When number of revolution is increased the apogee burn is split in shorter burn arcs. The mission becomes a A-A-P or a A-A-A-P.

The solution of the two-body problem was quite straight-forward and so the next step was the introduction of the perturbations due to the asphericity of the Earth. Even though the effect on the final mass is quite small, the zonal effect J2 changes the optimal deployment strategy, which now prescribes to first have a brief perigee burn and then a long apogee ones (see section 5.1.1). In this case the mission is a P-A (or P-A-A...). Even if there is a slight dependence on time with a 24-h cycle, the convergence was still straightforward. It was also relatively easy adding new revolutions around Earth.

A complex behavior rose with the introduction of the luni-solar perturbation. Once a solution is found for a departure date, convergence was sometimes not obtained when this solution was used as tentative guess for a different departure date. The perturbation at the apogee changes the orbit period and so the time of the perigee burn position is different from a departure day to another one. Also the solution is very sensitive to the perigee burn, even if it is very little. Also, as the initial

revolution period is modified, all the apogee burn times changed, even if they are longer and it was easier to get them. Often the time was completely misplaced and there were no way to get the solution without a manual changes of the guess solution. Unfeasible solutions with phases with negative length could also be obtained.

There were numerous tentatives, such as putting additional coast phases before and after the perigee arc to "catch" the shift of the time of the perigee time. A good tentative was to change the departure date gradually in order to have smooth behavior. But there were still two issues:

- to get the solution of a particular date it was necessary to explore all the solutions between the previous solution and the searched date
- Due to lunar perturbations, for multi-revolution mission, some arcs disappeared in certain date, in an unpredictable way.

To solve the problem of "'catching"' the perigee a change of variables was introduced. It was noted that, even if the burn times changed significantly changing the date, the right ascension of the burns were quite the same. So the new independent variables is ϑ and al the differential equation are changed multiplying time $\mathrm{d}t/\mathrm{d}\vartheta$ and changing the expression of the adimensional variable used for integration.

$$\varepsilon = j - 1 + \frac{\vartheta - \vartheta_{j-1}}{\vartheta_j - \vartheta_{j-1}} \tag{4.18}$$

In this way getting the initial guess solution was easier and if arcs were considered, the perigee arc is quite long, because the spacecraft is very fast at perigee and so sweeps a big angle in a short time. Inversion of times was solved and also the shifting of time. But still there was the problem of guessing the structure of the optimal solution.

For few revolutions (3.5 revolutions) exploring all the possible structures and taking only the optimal one was a feasible task. The solution can be a PAA, PA0 or P0A. The 0 indicated that the correspondent apogee burn is not present in the optimal solution for a certain departure date. For more revolutions it was not easy and also the problem was not scalable. After many trials, it resulted that to delete a burning arc was easier than adding one. So a continuation technique using perturbation fraction as parameter was introduced .

Starting from the J2 optimal solution with no other perturbations, all the burning arcs are present. In this case the perturbation fraction is $P_f = 0$. The perturbation fraction is inserted in the vector parameters $\boldsymbol{p}$. A new value of the perturbation fraction is inserted as boundary condition and the optimizer finds the new optimal solution. If the the optimal structure is the same (i.e. all the arcs are present) the convergence is straightforward and the new solution is memorized. The max value of switching function at each arc is also memorized. If an arc has to be deleted the

procedure does not converge, generally stopping for reaching max iterations number. This max iteration number is set to 30, providing sufficient margin, because, if the structure is already optimal, the procedure converges in 8-10 iterations. If the procedure does not converge the last converged optimal solution is taken and the minimum peak value of the Switching function indicates which arc has to be eliminated. So the structure is modified and the optimization is re-started. A new value of perturbation fraction is imposed as equality constraints until $P_f = 1$. The number of level of perturbations fraction is 6 for this problem and this continuation technique gets the optimal solution in the 98% of the solutions in a year (a solution for each different day). For having convergence in the remaing 2% it is sufficient to set more levels of perturbation fractions, because sometime a peak is lower than another, but it is growing or decreasing slowly. An improvement can be realized by evaluating the derivative of the Switching function value. When many revolutions are present (6.5 and more), more than one arc can be eliminated but often arcs are so small that different switching structures have very similar performance index.

4.4 Formation Flight

The single satellite optimization helped to understand the influence of the perturbation and also it was a good testbed to build a robust procedure for seeking the optimal solution and optimal structure. As said in Sec. 4.1 the two satellites have to reach the final orbit with a prescribed inter-satellite final distance. Only semimajor axis and eccentricity are specified for the final orbit, while the other parameters are free, but they have to be the same for both satellites.

In the final configuration the order of the satellites is not prescribed, so SAT1 can arrive first at the apogee or can arrive after SAT2. Both configurations have been explored. When a satellite arrives first at apogee it is designed as the formation leader, while the other one is called the follower. In this thesis two strategies are taken in consideration for reaching the final formation: chaser target and cooperative strategy.

In the Chaser-Target strategy the Target satellite applies its own optimal strategy, the same that is found in the single satellite optimization. The Chaser has to reach the same orbital parameter of the Target. It is important to note that Chaser - Target functions are different from Leader - Follower. The Chaser can be follower (arrive last at apogee) or Leader (arrive first), but it has to reach the same orbit that is optimal for the Target.

In the cooperative strategy the two satellites reach the same final orbit that is optimal for the formation and not only for the target. For the model point of view, the variables and the differential equations are the same for each satellite. So for the formation flight there are 28 state variables and 28 differential equations. The

Hamiltonian of the system is the sum of the Hamiltonian of the two satellites and each satellite has its own switching function.

In the formation flight there is also the constraint of the final intersatellite distance (phasing constraint). This constraint involves r, ϑ, φ of both satellites and so the optimal constraint should involve the adjoint variables of these quantities. It was noted that the distance between the two satellite is very small (10 km) and the two satellites have the same final orbit (because it is the final point). At the apogee the radius changes slowly, so it is possible to consider the radius equal for both satellite and so also the velocity is the same. Calling the velocity at the apogee V_A, the final distance d_f and considering velocity constant the final distance constraint can be written as

$$t_{f_F} = t_{f_L} + d_f/V_A \tag{4.19}$$

where the subscript F is for the follower, while L is for Leader. So the distance constraint is now a time constraint and prescribes the delay of the follower apogee arrival. The time constraint is easier to manage. The performance index is $\phi = m_{fS1} + m_{fS2}$.

4.4.1 Chaser Target

The Chaser Target strategy is the simplest, because the Target has to follow its own optimal solution and optimal strategy. The Chaser has to follow another optimal solution that is not the same of the single satellite case, because all the orbital parameters are now constrained. The boundary constraints for the Target are the same of the single satellite case (4.9-4.11).

$$\begin{aligned} r_f &= a(1+e) && (4.20)\\ u_f &= 0 && (4.21)\\ v_f^2 + w_f^2 &= (\mu/a)(1-e)/(1+e) && (4.22) \end{aligned}$$

while for the chaser one has

$$\begin{aligned} r_f &= r_T && (4.23)\\ \vartheta_f &= \vartheta_T && (4.24)\\ \varphi_f &= \varphi_T && (4.25)\\ u_f &= 0 && (4.26)\\ v_f &= v_T && (4.27)\\ w_f &= w_T && (4.28)\\ t_f &= t_T \pm d_f/V_A && (4.29) \end{aligned}$$

where the subscript f is for the final value of the chaser, while T is for the Target final value. The optimality boundary conditions for the target are

$$\begin{aligned} \lambda_{\vartheta f} &= 0 && (4.30)\\ \lambda_{\varphi f} &= 0 && (4.31)\\ \lambda_{vf} w_f - \lambda_{wf} v_f &= 0 && (4.32)\\ \lambda_{mf} &= 1 && (4.33) \end{aligned}$$

The final time is free, so the final Hamiltonian is null

$$H_f = 0 \tag{4.34}$$

The boundary conditions for optimality provide for the Chaser

$$\lambda_{mf} = 1 \tag{4.35}$$

For both satellites Hamiltonian continuity holds at the engine switching points; state and adjoint variables are continuous and, as a consequence, the switching function must be null there

$$S_{Fj} = 0 \qquad j = 1, \ldots, f-1 \tag{4.36}$$

In this way the Hamiltonian of the two satellites are separated; the convergence is easier and also the two problems can be solved in different times (first the trajectory of the Target and then the Chaser trajectory), and so the solution is faster. Both satellites can be Chaser or Target, but SAT1 is lighter and, with the same Thrust of SAT2, is more agile, so it is the most suitable to be the chaser, because can change the optimal trajectory of the single satellite case with less penalty than SAT2.

4.4.2 Cooperative strategy

With cooperative deployment both satellites modify their strategies in order to fulfill phase requirements saving the overall fuel. The optimization of the two trajectories has to be performed at the same time. The two satellites will have different times of switching on and off the engines. Also the strategies (number of coast and burn arcs) will be, in general, different (i.e. SAT1 PAA0 and SAT2 PA0A). It is convenient to split the trajectories of the two satellites in the same number of phases, each one described by the adimensional variable ϵ. Some of the phases will be constrained to zero-length (this constraint will replace the constraint of $S_F = 0$). This simplifies the problem description. The Boundary conditions involves both satellites

$$
\begin{aligned}
(r_{S1})_f &= a(1+e) && (4.37)\\
(u_{S1})_f &= 0 && (4.38)\\
(v_{S1})_f^2 + (w_{S1})_f^2 &= (\mu/a)(1-e)/(1+e) && (4.39)
\end{aligned}
$$

and

$$
\begin{aligned}
(r_{S2})_f - (r_{S1})_f &= 0 && (4.40)\\
(\vartheta_{S2})_f - (\vartheta_{S1})_f &= 0 && (4.41)\\
(\varphi_{S2})_f - (\varphi_{S1})_f &= 0 && (4.42)\\
(u_{S2})_f - (u_{S1})_f &= 0 && (4.43)\\
(v_{S2})_f - (v_{S1})_f &= 0 && (4.44)\\
(w_{S2})_f - (w_{S1})_f &= 0 && (4.45)\\
(t_{S2})_f - (t_{S1})_f &= \pm d_f/V_A && (4.46)
\end{aligned}
$$

The optimal boundary conditions are

$$
\begin{aligned}
(\lambda_{rS1})_f + (\lambda_{rS2})_f &= 0 && (4.47)\\
(\lambda_{\vartheta S1})_f + (\lambda_{\vartheta S2})_f &= 0 && (4.48)\\
(\lambda_{\varphi S1})_f + (\lambda_{\varphi S2})_f &= 0 && (4.49)\\
[(\lambda_{vS1})_f + (\lambda_{vS2})_f]\, w_f - [(\lambda_{wS1})_f + (\lambda_{wS2})_f]\, v_f &= 0 && (4.50)\\
(\lambda_{mS1})_f &= 1 && (4.51)\\
(\lambda_{mS2})_f &= 1 && (4.52)\\
(H_{S1})_f + (H_{S2})_f &= 0 && (4.53)
\end{aligned}
$$

At interior points, where engines are switched on or off, the switching function of both satellites is null. It is possible to see that the adjoint variables of the two satellites are no more independent.

The problem stated in this way has $(\lambda_m)_f = 1$ as final condition and λ_{m_0} as unknown parameter to be determined (for each satellite). But adjoint differential equations are homogeneous ($\boldsymbol{g}_\lambda(\boldsymbol{\lambda}) = 0$), so it is possible to scale all λ in order to have an easier BVP problem to solve. For the sake of clearness, the intermediate

passage are shown here. The original problem has

$$\begin{aligned} H_{S1} + H_{S2} &= 0 \\ \lambda_{m_0 S1} & \\ \lambda_{m_0 S2} & \\ \lambda_{m_f S1} &= 1 \\ \lambda_{m_f S2} &= 1 \end{aligned}$$

The Hamiltonians, and so the adjoint variables of each satellite, are scaled by factors K_1 and K_2.

$$\begin{aligned} H'_{S1} &= K_1 H_{S1} \\ H'_{S2} &= K_2 H_{S2} \\ \lambda'_{m_0 S1} &= K_1 \lambda_{m_0 S1} \\ \lambda'_{m_0 S2} &= K_2 \lambda_{m_0 S2} \\ \lambda'_{m_f S1} &= K_1 \lambda_{m_f S1} = K_1 \\ \lambda'_{m_f S2} &= K_2 \lambda_{m_f S2} = K_2 \end{aligned}$$

If $K_1 = 1/\lambda_{m_0 S1} = \lambda'_{m_f S1}$ and $K_2 = 1/\lambda_{m_0 S2} = \lambda'_{m_f S2}$

$$\begin{aligned} \lambda'_{m_0 S1} &= 1 \\ \lambda'_{m_0 S2} &= 1 \end{aligned}$$

the new scaled problem has two more initial conditions set and two less boundary conditions on the terminal point. All the others conditions are scaled as in this equation:

$$H'_{S1}/\lambda'_{m_f S1} + H'_{S2}/\lambda'_{m_f S2} = 0$$

4.5 Collision Avoidance

The Chaser Target and the cooperative Strategy prescribes only the final distance between satellites, but during the deployment the distance between them can vary. In order to prevent the collision between the two spacecrafts, the minimum distance has to be always greater than a safety value, that is 1 km. Using an indirect method it is not possible to put directly an inequality constraint. It is only possible to put an equality constraint when the inequality is active and this can be done only a posteriori.

It is possible to guess where the constraint can be violated: at the very beginning and in the last burn arc. At the very beginning it is the separation phase, so it is not

possible any control and everything is up to the separation stage of the launcher. During the last burn arc the distance can vary, but now the orbit of the two satellites are very close, so a collision can happen and collision avoidance constraint must be introduced. The additional boundary conditions enforce prescribed value d_{sep} and set the derivative of the distance to zero (because it has to be the minimum distance)

$$\begin{aligned}(\boldsymbol{r}_{S2} - \boldsymbol{r}_{S1})^T(\boldsymbol{r}_{S2} - \boldsymbol{r}_{S1}) &= d_{sep}^2 && (4.54)\\ (\boldsymbol{r}_{S2} - \boldsymbol{r}_{S1})^T(\boldsymbol{v}_{S2} - \boldsymbol{v}_{S1}) &= 0 && (4.55)\end{aligned}$$

The optimality conditions are derived using equations (2.35) and (2.36). All the adjoint variables have a discontinuity at the minimum distance (if constrained). Δ indicates the difference between values just after and before the minimum distance point.

$$\begin{aligned}\Delta\boldsymbol{\lambda}_{rS1}^T\boldsymbol{N} &= 0 && (4.56)\\ \Delta\boldsymbol{\lambda}_{rS2}^T\boldsymbol{N} &= 0 && (4.57)\\ \Delta\boldsymbol{\lambda}_{vS1}^T\boldsymbol{N} &= 0 && (4.58)\\ \Delta\boldsymbol{\lambda}_{vS2}^T\boldsymbol{N} &= 0 && (4.59)\\ \Delta\boldsymbol{\lambda}_{vS1}^T(\boldsymbol{v}_{S2} - \boldsymbol{v}_{S1}) &= 0 && (4.60)\\ \Delta\boldsymbol{\lambda}_{vS2}^T(\boldsymbol{v}_{S2} - \boldsymbol{v}_{S1}) &= 0 && (4.61)\\ \Delta\boldsymbol{\lambda}_{rS1}^T(\boldsymbol{r}_{S2} - \boldsymbol{r}_{S1}) &= \Delta\boldsymbol{\lambda}_{rS2}^T(\boldsymbol{r}_{S2} - \boldsymbol{r}_{S1}) && (4.62)\\ \Delta\boldsymbol{\lambda}_{vS1}^T(\boldsymbol{r}_{S2} - \boldsymbol{r}_{S1}) &= \Delta\boldsymbol{\lambda}_{vS2}^T(\boldsymbol{r}_{S2} - \boldsymbol{r}_{S1}) && (4.63)\\ \Delta\boldsymbol{\lambda}_{rS1}^T(\boldsymbol{v}_{S2} - \boldsymbol{v}_{S1}) &= \Delta\boldsymbol{\lambda}_{vS1}^T(\boldsymbol{r}_{S2} - \boldsymbol{r}_{S1})V_{rel}^2/d_{sep}^2 && (4.64)\\ \Delta\boldsymbol{\lambda}_{rS2}^T(\boldsymbol{v}_{S2} - \boldsymbol{v}_{S1}) &= \Delta\boldsymbol{\lambda}_{vS2}^T(\boldsymbol{r}_{S2} - \boldsymbol{r}_{S1})V_{rel}^2/d_{sep}^2 && (4.65)\end{aligned}$$

where $\boldsymbol{N}$ is the vector normal to both $\boldsymbol{r}_{S2} - \boldsymbol{r}_{S1}$ and $\boldsymbol{v}_{S2} - \boldsymbol{v}_{S1}$, and $V_{rel} = |\boldsymbol{v}_{S2} - \boldsymbol{v}_{S1}|$ is the magnitude of the relative velocity. From Eqs. (2.37) and (2.38) one also has an additional transversality condition

$$\Delta H_{S1} + \Delta H_{S2} = 0 \tag{4.66}$$

The boundary conditions are complex and involve all the variables (except mass and its adjoint). To find the optimal solution it is possible to start from an unconstrained solution and introducing $\Delta\lambda$ close to zero, but not exactly zero, in the tentative solution and adding the constraints.

It is possible to fulfill the collision avoidance constraint in a faster and simpler way. The idea is to constraint a difference in the last burn apogee. The value to use as difference is found with an an iterative procedure (few iterations of the

bisection methods). The last arc is split at the apogee, where the radial velocity is null ($u_{S1} = 0$, $u_{S2} = 0$). Then the difference of the apogee radius is enforced

$$r_{S1} - r_{S2} = d_{apo} \tag{4.67}$$

Since the state variable r is involved in an interior boundary constraint, the respective adjoint variable has a discontinuity.

$$\Delta\lambda_{rS1} + \Delta\lambda_{rS2} = 0 \tag{4.68}$$

derived by Eq. (2.35) and (2.36)

4.6 Optimal Constant-Direction Thrust

The optimal control theory gives the thrust magnitude and direction of the optimal solution for a given structure (number of coast and burn arcs). For this type of transfer, the thrust direction is mainly perpendicular to the line of apses, with little components out of plane or along apses. It was interesting to find how the final solution can be influenced optimizing only the duration of the arc burn and taking fixed the thrust angles. It was not only a theoretical curiosity, but also a practical issue. The physical model used for the trajectory optimization uses a point-mass spacecraft, but in the real world the satellite has momentum of inertia and all the changes in attitude require fuel. Also, changing attitude when the engine is on decreases the precision of the maneuver. Finding a control law that does not require much changing in thrust direction can be a first guess for an higher fidelity analysis.

A spacecraft is generally built to have the thrust direction for orbital maneuver mainly oriented along the spinning axis. This is essential for spinning satellites, but also for three axes stabilized ones. In case of emergency these spacecrafts enter in safe mode and start spinning.

So the best choice is to find a control law that keeps the thrust direction fixed in the inertial frame. During the j-th burn, thrust components in the geocentric inertial reference frame ($\boldsymbol{I}$, $\boldsymbol{J}$, $\boldsymbol{K}$) are written as

$$\begin{aligned} T_x &= T\cos\alpha_j\cos\beta_j && (4.69)\\ T_y &= T\sin\alpha_j\cos\beta_j && (4.70)\\ T_z &= T\sin\beta_j && (4.71)\\ & && (4.72) \end{aligned}$$

where α_j and β_j are the thrust angles. A simple change of reference frame provides the component in the topocentric frame $\boldsymbol{\imath}$, $\boldsymbol{\jmath}$, $\boldsymbol{k}$,

$$\begin{Bmatrix} T_u \\ T_v \\ T_w \end{Bmatrix} = \begin{bmatrix} \cos\vartheta\cos\varphi & \sin\vartheta\cos\varphi & \sin\varphi \\ -\sin\vartheta & \cos\vartheta & 0 \\ -\cos\vartheta\sin\varphi & -\sin\vartheta\sin\varphi & \cos\varphi \end{bmatrix} \begin{Bmatrix} T_x \\ T_y \\ T_z \end{Bmatrix} \tag{4.73}$$

So the thrust components in local frame T_u, T_v and T_w now depend also on the state variables ϑ and φ. The Euler-Lagrange equations for the corresponding adjoint variables have to be updated

$$\begin{aligned}
\dot{\lambda}_{\vartheta_T} &= [\lambda_u(T_x \sin\vartheta\cos\varphi - T_y \cos\vartheta\cos\varphi) \\
&+ \lambda_v(T_x\cos\vartheta - T_y\sin\vartheta) \\
&+ \lambda_w(-T_x\sin\vartheta\sin\varphi + T_y\cos\vartheta\sin\varphi)]/m \qquad (4.74)\\
\dot{\lambda}_{\varphi_T} &= [\lambda_u(T_x\cos\vartheta\sin\varphi + T_y\sin\vartheta\sin\varphi - T_z\cos\varphi) \\
&+ \lambda_v(0) \\
&+ \lambda_w(T_x\cos\vartheta\cos\varphi + T_y\sin\vartheta\cos\varphi + T_z\sin\varphi)]/m \qquad (4.75)
\end{aligned}$$

In this case $\Lambda_T \neq \lambda_V$ (see 4.3) and the general expression of the Switching function has to be taken in account.

First fixed values are considered for the thrust angles of the single satellite mission. For the shape of the initial reference orbit, that has the line of the apses along y axis and is coincident with the line of the nodes, $\alpha = 0$ and $\beta = -i_0$ (where i_0 is the inclination of the initial orbit) are adopted during the perigee burn, whereas $\alpha = \pi$ and $\beta = i_0$ are used during the apogee burns. This thrust vector lays on the orbital plane and it is always accelerating. Convergence to optimal solutions is easily achieved using the J2 solution as tentative guess. It can be used also as tentative guess the free thrust solution with perturbations.

The previous control law, with thrust angles decided a priori, is not suitable for more complex solutions, for example if the final orbital elements are fixed or if a change of plane is required. In this case study, having a cooperative deployment, it is not possible to achieve phasing and final orbit constraints. The two satellites are under different perturbations at different times and they have to reach the same final orbit.

The next mandatory step is to optimize not only the time of the burn arc, but also the thrust angle. The two thrust angles α and β remain fixed in the inertial frame during the burn arc, but they change from one arc to another. Optimal control theory is applied to determine the optimal thrust angles. Each thrust angle for each burn arc is a stand alone variable, but the variable are independent between them (they are not "'active"' at the same time) so they are stored in the same variable in the implementation. There will be the optimal thrust angles α_j and β_j and their adjoint variables $\lambda_{\alpha j}$ and $\lambda_{\beta j}$. For each j pair of angles there are the correspondent Euler-Lagrange equations $\mathrm{d}\lambda_{\alpha j}/\mathrm{d}t = -\partial H/\partial\alpha_j$, that is and $\mathrm{d}\lambda_{\beta j}/\mathrm{d}t = -\partial H/\partial\beta_j$

$$\dot{\lambda}_\alpha = -\frac{T}{m}\left(\lambda_u\frac{\partial(T_u/T)}{\partial\alpha} + \lambda_v\frac{\partial(T_v/T)}{\partial\alpha} + \lambda_w\frac{\partial(T_w/T)}{\partial\alpha}\right) \qquad (4.76)$$

$$\dot{\lambda}_\beta = -\frac{T}{m}\left(\lambda_u\frac{\partial(T_u/T)}{\partial\beta} + \lambda_v\frac{\partial(T_v/T)}{\partial\beta} + \lambda_w\frac{\partial(T_w/T)}{\partial\beta}\right) \qquad (4.77)$$

The partial derivative of the cosines director of the with respect to α and β are:

$$\begin{Bmatrix} \frac{\partial(T_u/T)}{\partial\alpha} \\ \frac{\partial(T_v/T)}{\partial\alpha} \\ \frac{\partial(T_w/T)}{\partial\alpha} \end{Bmatrix} = \begin{bmatrix} \cos\vartheta\cos\varphi & \sin\vartheta\cos\varphi & \sin\varphi \\ -\sin\vartheta & \cos\vartheta & 0 \\ -\cos\vartheta\sin\varphi & -\sin\vartheta\sin\varphi & \cos\varphi \end{bmatrix} \begin{Bmatrix} -\sin\alpha\cos\beta \\ \cos\alpha\cos\beta \\ 0 \end{Bmatrix} \tag{4.78}$$

$$\begin{Bmatrix} \frac{\partial(T_u/T)}{\partial\beta} \\ \frac{\partial(T_v/T)}{\partial\beta} \\ \frac{\partial(T_w/T)}{\partial\beta} \end{Bmatrix} = \begin{bmatrix} \cos\vartheta\cos\varphi & \sin\vartheta\cos\varphi & \sin\varphi \\ -\sin\vartheta & \cos\vartheta & 0 \\ -\cos\vartheta\sin\varphi & -\sin\vartheta\sin\varphi & \cos\varphi \end{bmatrix} \begin{Bmatrix} -\cos\alpha\sin\beta \\ -\sin\alpha\sin\beta \\ \cos\beta \end{Bmatrix} \tag{4.79}$$

According to these equations the $\lambda_{\alpha j}$ and $\lambda_{\beta j}$ are always null except in the $j-th$ arc and so the optimal boundary conditions are

$$\lambda_{\alpha_j} = 0 \qquad j = 1,\ldots,f-1 \tag{4.80}$$

$$\lambda_{\beta_j} = 0 \qquad j = 1,\ldots,f-1 \tag{4.81}$$

at the beginning and at the end of the arc. The free-thrust direction solution is used as tentative guess with $\alpha_j = 0$ or π and $\beta_j = \pm i_0$ in agreement with the previous observations.

4.7 Errors in control law

The mission of deployment of the two satellites in formation flight can be accomplished with optimal variable angles or with fixed ones for each arc. The one with fixed angles is the one more suitable for a real flying mission. But real missions are subjected to errors with respect to the optimal trajectory.

The errors can be classified in three main categories: errors due to the approximation of the dynamic model, errors due to the orbit determination (state of the spacecraft at a certain moment) and errors due to actuation. These errors cannot be avoided, and are part of the problem, but their influence can be mitigated improving precision in models, actuation and sensor but also designing a robust mission where handling and recovering errors is possible.

In this thesis the model and orbit determination errors are not considered, and only errors in controls implementations are taken into account. In the mathematical model considered here, thrust can vary between a maximum value T_{max} and minimum value 0. The optimal control theory states that a bang-bang control is optimal and the optimal direction is parallel to the primer vector $\boldsymbol{\lambda}_V$ when thrust direction is free. For constant-direction thrusting optimal thrust angle is found for

each arc. This is indicated as nominal thrust $\boldsymbol{T}_N$. The real thrust vector is actually $\boldsymbol{T}_R = \boldsymbol{T}_N + \boldsymbol{T}_\epsilon$, where $\boldsymbol{T}_\epsilon$ is the thrust error vector.

The real vector $\boldsymbol{T}_R$ is inside a cone around $\boldsymbol{T}_N$. The magnitude is expressed as $T_R = T_N + \Delta T$ and the position of the vector in Cartesian coordinates is

$$\begin{Bmatrix} T_x \\ T_y \\ T_z \end{Bmatrix} = \begin{bmatrix} \cos\alpha\cos\beta & -\sin\alpha & \cos\alpha\sin\beta \\ \sin\alpha\cos\beta & \cos\alpha & \sin\alpha\sin\beta \\ \sin\beta & 0 & \cos\beta \end{bmatrix} \begin{Bmatrix} T_R\cos\gamma \\ T_R\sin\gamma\cos\delta \\ T_R\sin\gamma\sin\delta \end{Bmatrix} \tag{4.82}$$

where γ is the angular distance between the nominal thrust vector and the real one. It is the amplitude of the cone where the real thrust vector lays. δ gives the position on the cone surface.

Finding an optimal solution is not enough, but also a robust solution is pursued. The methods found in literature involve generally MonteCarlo simulation and genetic algorithms. The method that seems more suitable with the optimization indirect method it is the reduction of covariance matrix described by Zimmers in [69]. The approach followed in this thesis was more empiric, but these results were kept in consideration. Errors in orbit determination are not taken in consideration, so the approach is more focused on the strategy that mitigates effects of actuation errors.

The control law with fixed thrust angles for each different arc was the starting point. Errors in thrust magnitude and directions are introduced. The errors are simulated using random generator function in Fortran. The results is a thrust profile with a constant component (different for each arc) plus a white noise component. The errors on the thrust magnitude and on γ are simulated with a Gaussian distribution, while δ is generated with uniform distribution.

First, the influence of errors on the final constraints is evaluated in an open-loop simulation. Then in order to mitigate the errors on the final constraint, an updated control law is devised. A mission with random error is simulated and, after each revolution, an observation is taken to track the satellite. By considering this position as the real one, the remaining mission is re-optimized. This approach emulates a Model predicted control (MPC), were the optimizer models and designs each step of the mission, while the injection error subroutine simulates a real mission behavior.

This concept had some convergence problem, because the errors change state and adjoints variables values. The errors change r_a and r_p and can modify sensibly switching structure and thrust angles, requiring a solution far from the nominal one. So a different procedure that keeps the same switching structure was introduced: the final arc width is fixed and has a low value τ_s. This additional boundary condition substitutes the $SF = 0$ condition for the final arc. This condition is eliminated only for the final re-optimization. The time length of final burn arc is fixed, that is, if only a satellite is considered,

$$t_{(f-1)} - t_{(f-2)} = \tau_s \tag{4.83}$$

If the the formation deployment is considered

$$t_{(f-1)_{S1}} - t_{(f-2)_{S1}} = \tau_s \tag{4.84}$$
$$t_{(f-1)_{S2}} - t_{(f-2)_{S2}} = \tau_s \tag{4.85}$$

This constraint on time requires continuity in the Hamiltonian, so for a single satellite deployment is

$$\Delta H_{f-2} = H_{(f-2)+} - H_{(f-2)-} = 0 \tag{4.86}$$

and for a formation deployment is

$$H_{(f-2)+_{S1}} - H_{(f-2)-_{S1}} = 0 \tag{4.87}$$
$$H_{(f-2)+_{S2}} - H_{(f-2)-_{S2}} = 0 \tag{4.88}$$

Conclusions

The boundary conditions for single satellite or formation satellite deployment have been given. Tranversality and optimality conditions have been derived in the frame of the OCT. The optimal control is a bang-bang thrust with direction parallel to the primer vector. During the study of the optimal transfer of the single satellite with luni-solar perturbations, a procedure that gradually introduces these perturbations has been developed for increasing problem convergence. In the chaser-target deployment optimality and transversality conditions of the two satellites are decoupled, while they are linked together in the cooperative deployment. Two collision avoidance boundary conditions are shown. An alternative sub-optimal control law with thrust direction fixed in the inertial frame is used. Finally thrust dispersion errors are injected in the previous approximate control law, suggesting a robust re-optimization strategy with a short-time final arc.

Chapter 5

Numerical Results

Introduction

The indirect optimization method is applied to the deployment of the satellite formation. First the single satellite behavior is analyzed considering the influence of thrust level and number of revolutions. Then the Earth oblateness, Moon and Sun perturbations are introduced and the results on the final mass, thrust angles and strategy (number, duration and sequence of thrust arcs) are shown. The same procedure is applied to the formation deployment. The strategy for collision avoidance is also analyzed. An approximate control law with thrust direction fixed in the inertial frame is considered and finally the robust re-optimization strategy results are shown.

5.1 Single Satellite Deployment

The deployment of a single satellite named SAT0 with initial mass $m_0 = 960Kg$ is first considered. All the details of the case study are exposed in chapter (4.1). As reminder, in the first revolution and at the last apogee no maneuvers are allowed. The initial orbit is the reference one. The deployment uses the dynamical model described in chapter 3 with the indirect method explained in section (2.4). The reference engine has thrust of $T = 8N$, but to better understand the influence of thrust magnitude also $T = 1N$ is considered. The time of the deployment is not a constraint, so missions with length ranging from 2.5 (the minimum possible) to 6.5 revolutions around the Earth were analyzed. The reference case was considered the 4.5-revolution mission that seemed the best compromise between performance index and time of deployment.

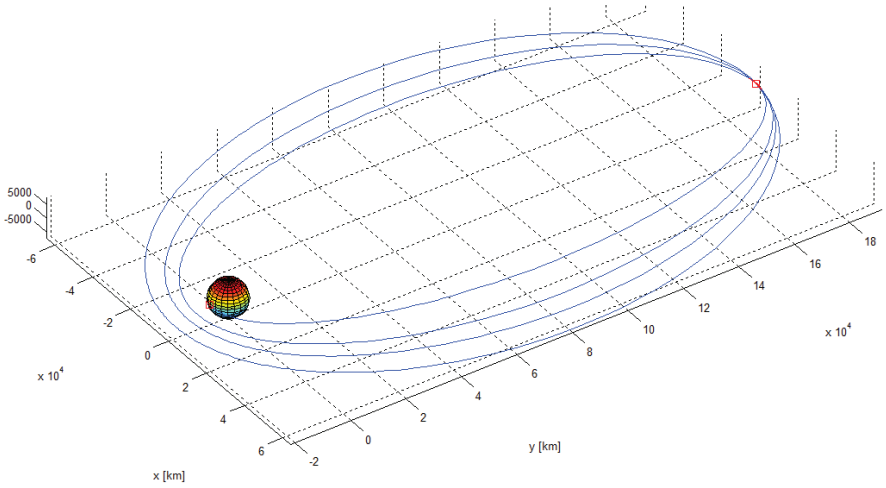

Figure 5.1: Trajectory plot

5.1.1 J2 solutions

The deployment of a single satellite in a high elliptic orbit from reference orbit A to final orbit B, see Fig. (5.1), is mainly a perigee raising with a little decrease of the apogee. Only final semimajor axis and eccentricity are constrained. In a two impulsive manoeuvre (in 2.5 revolutions) without perturbations the deployment can be performed and a big $\Delta \boldsymbol{V}$ would be placed at the apogee for accelerating the spacecraft whereas a little one will be placed at the perigee to decelerate and lowering the apogee. For energetic reasons the optimal strategy sequence will be A - P (see [68]), that means coast revolution before the first burn at apogee and then a perigee burn. The final point is the following apogee. This synthetic script will be used along the text and it will indicate the position of the burns and their sequence, describing the optimal strategy.

The satellite is injected at the perigee of the initial orbit by the launcher. If the J2 model is considered, perturbations of the bulge of the Earth modify the reference orbit, decelerating the spacecraft and so lowering the apogee height. The J2 perturbations have a null effect on the semimajor axis when a complete revolution is performed, but the deployment mission is always $n+1/2$ revolutions, so the effect is not more null. The main effect is to change the orbit transfer from a perigee rising - apogee lowering to a perigee - apogee rising. The maneuver at the perigee is still little, but now it accelerates the spacecraft. Also the optimal strategy changes from a A - P to a P - A.

Even if it is possible to still have a A - P strategy and having a sub-optimal solution, the indirect method optimization has difficulties in convergence and, as

final results, always show $S_F > 0$ at the first perigee; this fact shows that a burn could improve the solution.

It is worth to say that the optimal solution generally requires burn arcs at the beginning and at the end of the mission, but as said in the previous chapter, these maneuver are not allowed for operational reasons.

If impulsive manoeuvres are considered it does not matter how may revolutions are performed. The manuevers occur perfectly at the apogee or perigee, without losses, and if the perigee raising is split in more revolutions, the performance index does not change. If finite thrust is considered, gravitational losses are present and grow as the angular length of the burn is increased (thrust applied farther from the apsis). This means that a long arc will have more losses than a short one. As expected, higher thrust means shorter arc and so better final mass. But with the same level of thrust the final mass can be improved with multiple revolution. In this way the burn is split in shorter arcs with lower losses. So the P - A mission will become a P - A - A - etc.

Even if in terms of time or angle, splitting also the perigee manoeuvre in more arcs is possible, in this case the perigee burn is so little that does not affect the final mass and, for the optimal strategy, it is better performing all the perigee maneuver before apogee one. The benefits on the performance index deriving from multi-revolutions are more evident when the thrust level is lower (Fig. 5.2). A larger number of burn arcs is also preferred as they allow an easier corrections of the errors that may occur during the maneuvers.

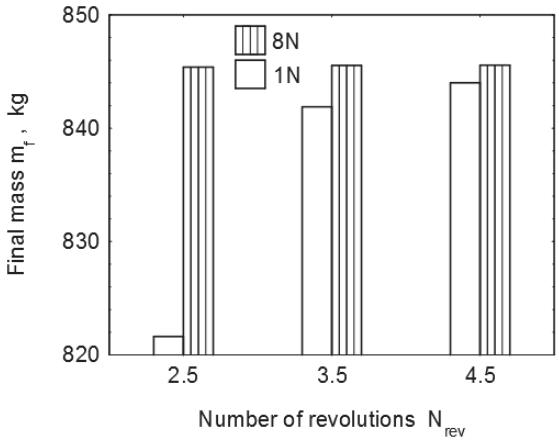

Figure 5.2: Comparison between mission with different number of revolutions using 1N or 8N thrust level

Table 5.1 gives some details of these maneuvers. The length of each maneuver can be expressed in time or in angle. Both descriptions are useful and give different

information. Time length is linked to propellant mass expulsed by the spacecraft. The width of the arc gives an idea of the loss (wider is the arc, higher the losses are), but it is important how much time the spacecraft is thrusting far from the perigee/apogee. For example the perigee arc is wider than the apogee one, but, because of the high eccentricity, the time spent at the perigee is little. When more revolutions are considered the ΔV of the apogee maneuver is split in more arcs. As one can see from Tables 5.1, the time length of the single arc decrease at every passage ($\Delta t_{A3} < \Delta t_{A2} < \Delta t_{A1}$) because the optimization tries to have a uniform split of the ΔV among the arcs. As the spacecraft becomes lighter after each burn, the thrust acceleration increases and the time for the same ΔV decreases. It is worth noting that velocity is larger at each later apogee (i.e. $V_{A2} > V_{A1}$) and so the angle A2 arc length is larger than A1 even if the time arc is shorter. The effect is more evident with lower thrust.

With more revolutions the perigee time length increases. Even if this can seem counter-intuitive, it can be understood looking at Figure 5.3. When 2.5 revolution mission is performed the A1 apogee burn is so long that it can increase also the apogee r_A, whereas in Figure 5.4 the apogee raise was given only by the perigee manuever. In these figure it is also possible to see the effect of J2 perturbation in lowering the apogee, and the "peaks" at every perigee that become smaller as the distance from Earth increases. It was expected that the optimal structure (a perigee

Table 5.1: Time and angular length of each burn (J2 only).

$T = 1$ N						
N_{rev}		P1	A1	P2	A2	A3
2.5	Δt, h	2.66	76.50	3.77	-	-
	$\Delta\vartheta$,deg	250.15	58.73	154.38	-	
3.5	Δt, h	0.45	35.55	-	34.79	-
	$\Delta\vartheta$,deg	121.27	18.40	-	23.15	-
4.5	Δt, h	0.65	23.28	-	22.95	22.63
	$\Delta\vartheta$,deg	152.88	10.90		12.97	15.02
$T = 8$ N						
N_{rev}		P1	A1	P2	A2	A3
2.5	Δt, h	0.09	8.50	-	-	-
	$\Delta\vartheta$,deg	28.50	4.67	-	-	-
3.5	Δt, h	0.09	4.29	-	4.20	-
	$\Delta\vartheta$,deg	28.97	2.04	-	2.61	-
4.5	Δt, h	0.09	2.87	-	2.83	2.79
	$\Delta\vartheta$,deg	29.05	1.30	-	1.55	1.80

with subsequent apogee manuevers) will be kept by different number of revolutions and with different thrust level.

As one can see in table 5.1 and in Figure 5.5 that one of the missions has two perigees maneuver. This happens because the thrust is so low that the apogee arc is too wide and the engine has not enough time to perform the perigee raising. So, the optimal strategy is to raise the first apogee in order to have more time to perform the perigee raising. Now the apogee maneuver can raise the perigee, but the arc is so wide that that the burn raises also the apogee. It needs then another perigee manuever to decrease r_A to the required value.

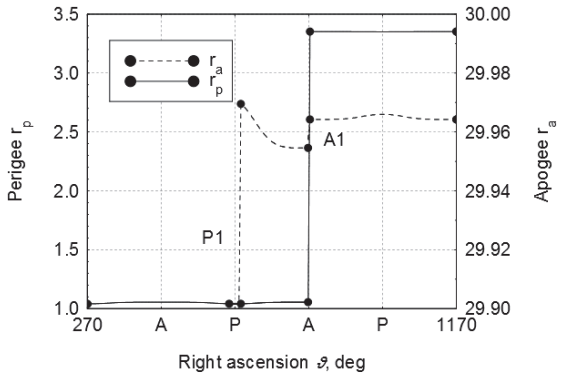

Figure 5.3: r_p and r_a during a 2.5-revolution mission, 8N thrust

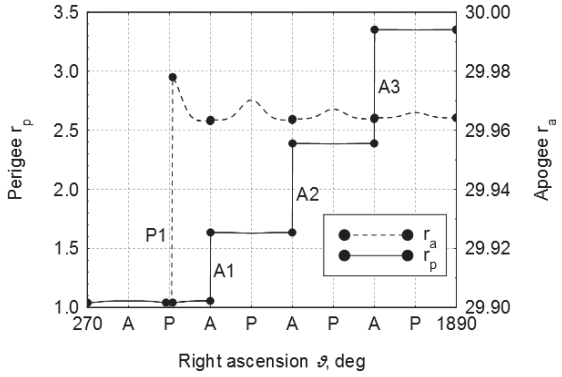

Figure 5.4: r_p and r_a during a 4.5-revolution mission, 8N thrust

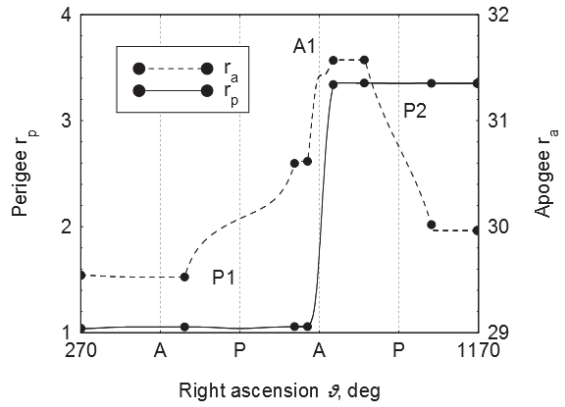

Figure 5.5: r_p and r_a during a 2.5-revolution mission, 1N thrust

5.1.2 Luni-Solar perturbations

Next step is introducing luni-solar perturbations. Also solar radiation pressure is considered in the simulation, even if it does not show significant effects. On the contrary the Moon and the Sun have a great influence on the final mass of the spacecraft, but also on the optimal strategy (sequence of perigee-apogee burn arcs and coast ones). The continuation technique to obtain converged solutions is explained in details in section 4.3. A solution with only J2 perturbations is the tentative guess solution, with all arcs. Perturbations are increased and, if a solution does not converge, the arc with the lowest peak value of the switching function is deleted. The entire procedure requires less than 50 iterations for convergence when no arc are deleted, while 80 iterations with one arc canceled. On a a Quad core intel i7 it takes 60 seconds (no parallelization, so only one core is used). The procedure is iterated for each day of the 1-year launch window starting December 1, 2015 (MJD 57357). In Figure 5.6 it is possible to see the final mass graph as a function of the departure date for the 4.5-revolution mission during the year. The difference between the highest and the lowest final mass is about 8 kg, showing how much studying this kind of perturbations is important. Another issue about lunar perturbation is that in the first revolution no maneuver are permitted and, if the Moon is an unfavorable position at the first apogee, the spacecraft plunges in the atmosphere. The position of the Moon depends on the departure date. In the figure it is possible to see two periodic contributions: the one with the lower frequency is the sun perturbation, while the other one is the Moon influence. The solar perturbation has a biggest effect on the final mass, but the Sun position is almost constant during the mission time, while the Moon moves of about 40-55 degrees for each spacecraft revolution. The variation of the angular displacement is due to eccentricity and to orbital period

changing of the spacecraft for the apogee burns.

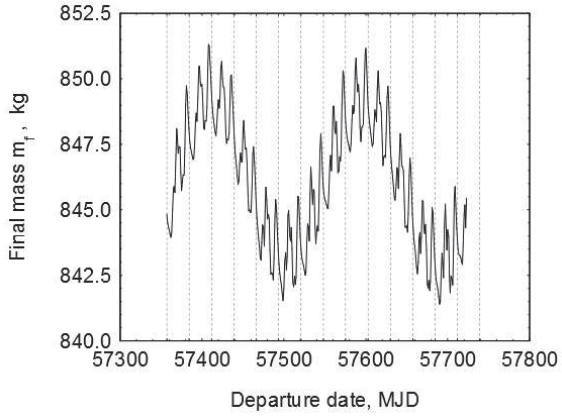

Figure 5.6: Final mass with departure date along 2016

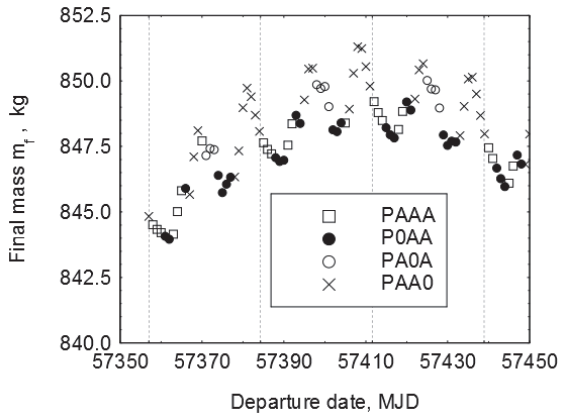

Figure 5.7: Final mass and switching function from December 2015 to February 2016

In Figure 5.7 the structure of the optimal solution is shown for each day from 1st December 2015 to the end of February for the 4.5-revolution solution. The problem was to understand why and when the optimal structure changed and the performance was so different. In simulation with almost circular orbit the Luni-solar perturbations do not seem to influence so much the semi-major axis, but in these case the high eccentricity changes the symmetry of the perturbations. Perturbations are markable at the apogee only, because it is far from the Earth. A first approach was to find the favorable positions of Moon and Sun considering that the most

important contribution is the tangential component of the perturbation that acts when the spacecraft is at the apogee. An approximate model was developed. If coplanar orbits are considered, the tangential component is

$$a_t = -\frac{\mu_b}{r_b^2}\left[(r_b/R)^3 - 1\right]\cos\vartheta_b \tag{5.1}$$

with the spacecraft distance from the perturbing body expressed as

$$R^2 = r_b^2 + r^2 - 2r_b r\sin\vartheta_b \tag{5.2}$$

and ϑ_b is the right ascension of the perturbing body. When the Sun is the perturbing body, $r << r_b$ and only first order terms are retained to obtain $(r_b/R)^3 \approx 1 + 3(r/r_b)\sin\vartheta_b$ and

$$a_t \approx -\frac{\mu_b}{r_b^2}\frac{3}{2}\sin(2\vartheta_b) \tag{5.3}$$

with maximum positive values at $\beta = 135$ and 315 deg (the most favorable positions of the Sun), and maximum negative values at $\beta = 45$ and 225 deg (the most unfavorable positions). If short-period oscillations due to the lunar gravity are ignored (two cycles are found in each sidereal period of the moon), the final mass in Fig. 5.6 closely follows this trend, with two sinusoids in the 1-year launch window. The peak values occur for departure on January 24, 2016 (MJD 57411, right ascensions of the Sun at departure and arrival are 307 and 323 deg) and July 27 2016 (MJD 57596, 127 and 143 deg).

When the Moon is considered, the spacecraft distance from the Earth becomes comparable to the Earth-Moon distance ($r/r_b \approx 0.5$) and the previous simplification does not hold. The symmetry of the result with respect to the x axis is broken and the effects of the third-body perturbation are enhanced when spacecraft apogees and Moon are on the same side with respect to the Earth, that is when $\sin\vartheta_b > 0$. The maximum benefit occurs when $\vartheta_b \approx 115$ deg (with a less pronounced beneficial effect at $\vartheta_b \approx 330$ deg), whereas the largest negative effect is at $\vartheta_b \approx 65$ deg (with a less remarkably effect at $\vartheta_b \approx 210$ deg). As said before, the Sun position during transfer mission does not change, so to verify the previous assessment for Moon favorable positions, the position of the Moon was considered fixed during the transfer and the Sun perturbations were neglected. As expected, in Figure 5.8, when th Moon is in a favorable position, the spacecraft exploits at every revolution the perturbation of the Moon to increase its velocity and save fuel. The longest mission (4.5 revolutions) can exploit significant lunar assist during five passages, two more than in the shortest ones: variations of the final mass with respect to the average value show roughly the same 5/3 ratio.

When Moon movements is involved, the case is more complex. Even if Sun perturbation is neglected the perturbation effects final mass that can be seen in

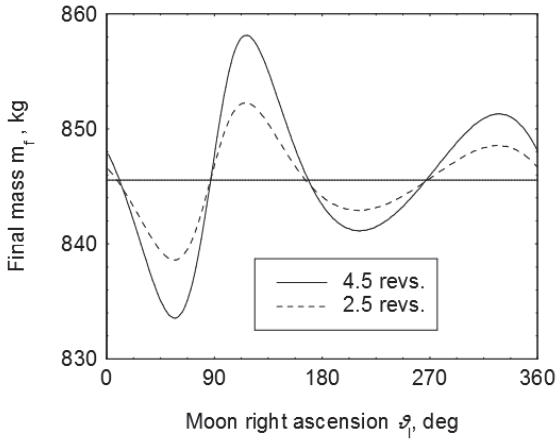

Figure 5.8: Lunar perturbations on final mass considering Moon position fixed

Figure 5.9 are not easy to be predicted. The Moon moves of 40-55 degrees during every revolution of the spacecrafts.

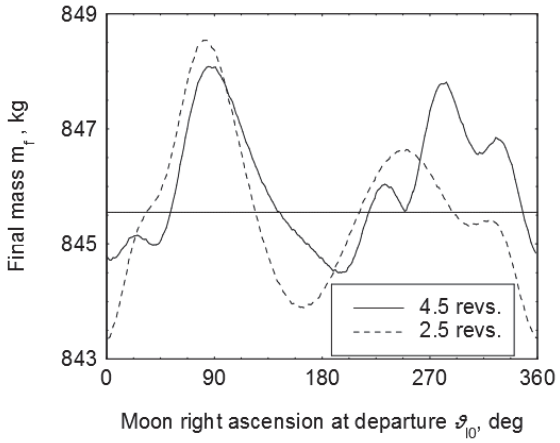

Figure 5.9: Lunar perturbations on final mass considering Moon motion

The Moon is at the most favorable position ($\vartheta_b = 115$ deg) at the first apogee passage of the best 2.5-revolution transfer, offsetting the penalty at the last one (205 deg). On the contrary, the worst performance occurs when the three apogee passages find the Moon at about 20, 70 and 125 degrees, with the most unfavorable configuration at the second passage.

The Moon moves about 210 degrees during the best 4.5-revolution transfer and is in a favorable position at the first (115 deg) and last (about 305 deg) apogee

passage (with a single unfavorable position, at about 205 degrees, during the third passage). However, the spacecraft adjusts the burn lengths and varies the orbital period during each revolution to put forward or push back the passages in order to enhance/reduce the effects of favorable/unfavorable geometrical configurations. On average, the final mass is larger in comparison to the shortest transfers, but the maximum achievable mass is lower.

The switching structure of the optimal 4.5-revolution missions (see Fig. 5.7) changes with a clear regularity according to the departure date. The best missions require the removal of the last burn arc (PAA0), whereas the removal of the first arc (P0AA) is beneficial in the worst cases. Optimization prescribes the removal of the last two arcs in four cases, and the switching structure becomes PA00. The same optimal structures repeat at roughly 14-day intervals, corresponding to a half revolution of the Moon around the Earth. For an assigned departure date, the thrust strategy has almost no capability of phasing the initial apogee passage with the Moon position. However a longer thrust arc at the first apogee increases the total time of flight. On the contrary, when the first apogee burn vanishes, the following orbital periods are shorter and the whole mission is faster. The trip time may differ more than 12 hours (about 6 degree in angular position of the Moon). Figure 5.10 shows that the mission departing on Dec. 12 delays the last apogee passage to find the Moon in a more favorable position. On the contrary, but with a similar aim, the mission starting on Dec. 5 anticipates the fourth apogee passage. Moon's complex influence on the spacecraft trajectories suggests that further analyses could provide interesting hints for all the missions that exploit lunar resonance.

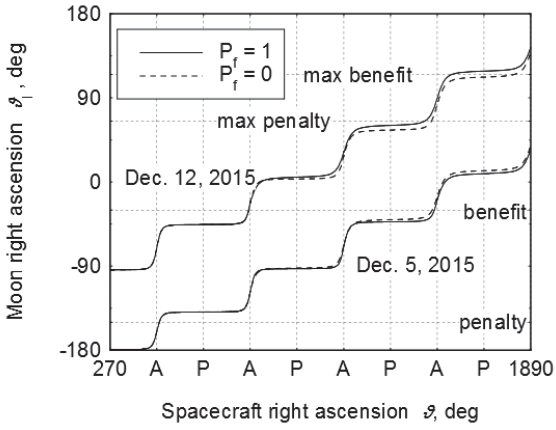

Figure 5.10: Spacecraft right ascension ϑ deg

If more revolutions are performed (see Figure 5.11) the average final mass is higher and there is a jump in the maximum mass due to the number of favourable

positions that the spacecraft can meet during its mission.

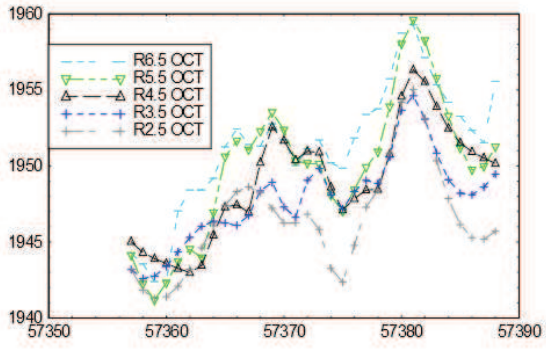

Figure 5.11: Total mass [kg] of the two satellites deployed individually

5.1.3 Example Case Analysis

The mission with departure on December 1 , 2015 is taken as example to show the details of the mission and the convergence procedure. Table 5.2 shows the time arc length of the 4.5-revolution mission with different perturbation levels. When $P_f = 0$ the arc lengths are almost the same and in Figure 5.12 the value of the switching function for each arc is represented using the adimensional variable ϵ. This representation has been chosen for the sake of clarity. Using t the perigee arc would be to little, while using ϑ the apogee arcs would be to little.

Table 5.2: Characteristics of the 4.5-rev. transfer with departure on Dec. 1, 2015.

P_f	$t_2 - t_1$ hr	$t_4 - t_3$ hr	$t_6 - t_5$ hr	$t_8 - t_7$ hr	m_f kg
0.0	0.09	2.87	2.83	2.79	845.57
0.2	0.09	3.59	2.75	2.16	845.40
0.4	0.09	4.27	2.79	1.45	845.25
0.6	0.09	4.97	2.96	0.59	845.10
0.8	0.09	5.51	3.02	-	844.96
1.0	0.09	5.84	2.70	-	844.83

The odd arcs represent coasting, while the even ones are the Thrusting arcs. The S_F is greater than zero also at the beginning and at the end of the mission, but no manuevers are allowed for operational constraints. For this departure date, when the perturbations fraction is increased the first arc becomes more convenient,

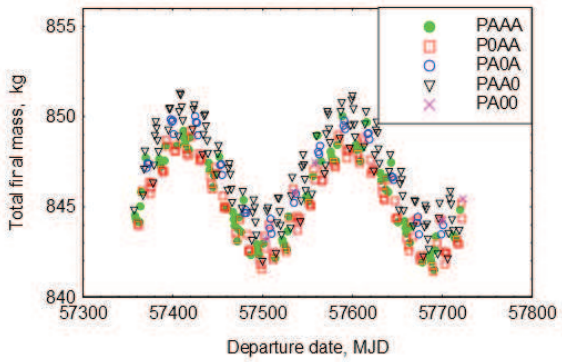

Figure 5.12: SAt0 Switching structure

increasing the time of flight of the mission. S_F peak increases and so does the time arc length. On the other hand the last arc becomes shorter. The switching function remains the same until $P_F = 0.6$. When the perturbations are increased to $P_F = 0.8$ with the same switching structure, the optimizer cannot fulfill the constraint $S_F = 0$ at the boundary of the last burn arc.

As the structure brings to an unfeasible solution the procedure comes back to the last converged solution at $P_F = 0.6$, where the lowest peak of the Switching Function is in the last arc. So the optimal structure is changed in P-A-A-0 and the optimizer converges now to an optimal solution. Pontryagin Maximum Principle (PMP) is satisfied and this assure the optimality, at least locally. This structure is kept until $P_F = 1$. Figure 5.13 shows the thrust angle values for each thrust arc.

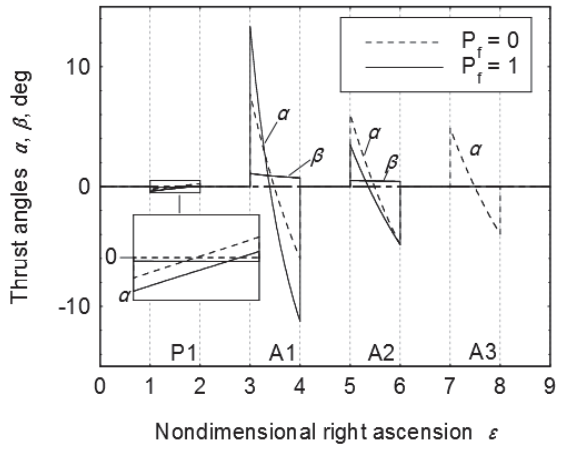

Figure 5.13: Thrust angles of 4.5-revolution mission

The in-plane thrust angle α is the angle between the spacecraft velocity and the projection of the thrust on the orbit plane (positive values correspond to thrust towards Earth), whereas the out-of-plane angle β is the angle between the thrust vector and the x-y plane. When all perturbations are considered there is a little out of plane component to change the plane and improve the benefit of the luni-solar gravitational perturbations. In the orbit plane, the thrust is directed inward with respect to the Earth when the spacecraft is moving outward ($0 < \nu < 180$ deg, that is, after perigee and before apogee) and vice-versa, to reduce the orbit eccentricity in agreement with the variational equations for orbital parameters [57]. Fig. 5.14 shows the variation of the final value of the orbital parameters Ω, ω, i.

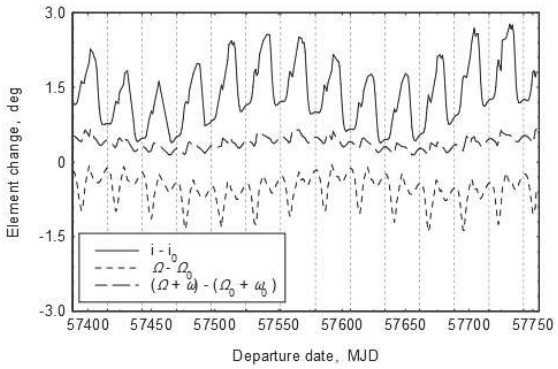

Figure 5.14: Final orbital elements

5.2 Chaser-Target and Cooperative deployment

The study of formation deployment is carried on for 4.5 revolutions and $T = 8N$. The two satellites SAT1 and SAT2 introduced in chapter 4.1 are injected in almost the same initial orbit by the launcher and they have to reach the final orbit with a final distance constraints that can be handled as a phasing constraint. All the procedure developed for the single satellite is valid for the formation flight. The main difference is that SAT2 is heavier, so it has a lower acceleration and the thrust arc are longer than for SAT1 and they disappear less frequently.

Formation deployment is first analyzed without the phasing constraint to highlight the difference behavior of the satellites, which are free to follow their own optimal strategy. They can have different optimal structures (different number of burn arcs) but from the implementation point of view, they have the same number of phases, some of them with time length equal to zero (Fig. 5.16,5.17). This approach is consistent with the procedure of finding the optimal structure increasing

the perturbations level. The integration of differential equations are carried on at the same time using the adimensional variable ϵ. In this way the two satellites can switch on and off the thruster at different times, even if the integration is taken in parallel (Fig. 5.15).

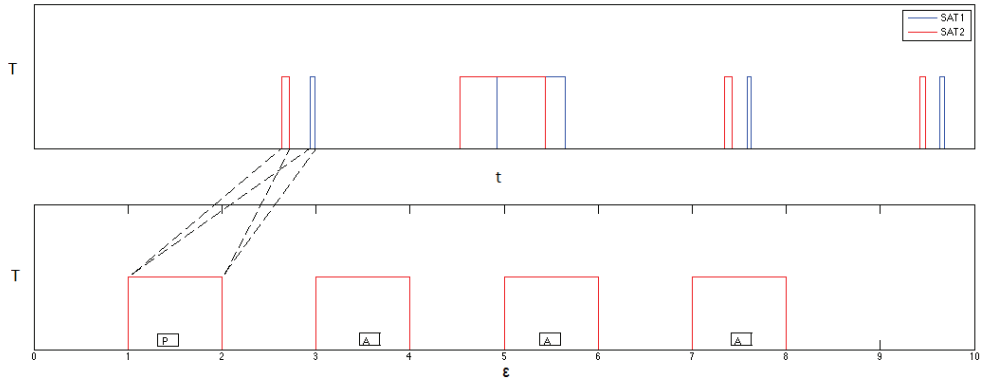

Figure 5.15: Thrust profile. On the top: time t. In the bottom: adimensional time ϵ

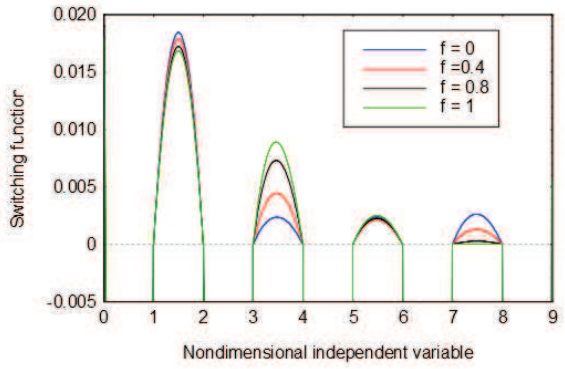

Figure 5.16: Switching Function SAT1

First the behavior of the two satellites can be analyzed when only the J2 perturbation is considered and the phasing constraint is neglected. SAT1 has a ΔV for separation and so has a higher energy orbit. The ΔV gives more velocity to SAT1 which is ahead of SAT2 at the beginning of the mission, but it has also a lower average angular velocity, so it is soon overtaken by SAT2 during the first revolution. At the following perigee SAT2 has gained 600 km with respect to SAT1. After the

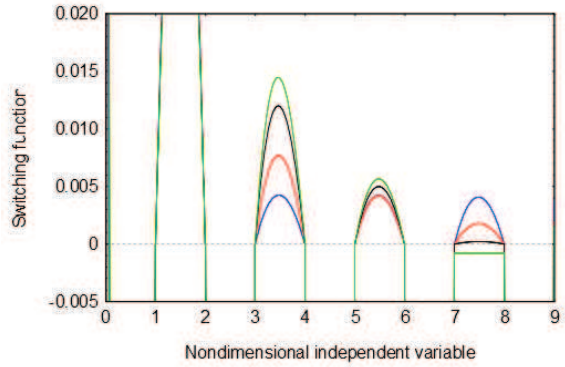

Figure 5.17: Switching Function SAT2

Table 5.3: Performance for different deployment strategies (J2 model, 1 N thrust).

Strategy	$(m_{S1})_f$	$(m_{S2})_f$	$(m_{S1})_f + (m_{S2})_f$
unconstrained	844.233	1097.443	1941.676
chaser-target SAT2 ahead	844.202	1097.443	1941.646
chaser-target SAT1 ahead	844.202	1097.443	1941.645
cooperative SAT2 ahead	844.219	1097.437	1941.656
cooperative SAT1 ahead	844.219	1097.436	1941.655

first perigee burn they reach almost the same energy. They follow their own optimal strategy and the ΔV of every single arc are similar between the two satellites. But the delay of the first revolution remains for all the mission. Because the velocity at the apogee increases, the time delay increases the relative distance that arrives at the end with a large final value (above 4000 km), with SAT1 following SAT2. The aim of the deployment is instead to take the two satellites to the final orbit with a final relative distance of 10 km at the apogee. After that, sensors can see the other spacecraft and they can start the close-approach manuever.

The arriving order is not a requirement, so SAT1 can be the leader (arrives first at the apogee) or the follower (arrives second). An approach for fulfilling the final constraint is the Chaser-Target. As already said in section 4.4.1, the target has its own optimal strategy, the same if it were a single satellite, while the chaser has to reach the same final orbit of the Target. It is important to avoid confusion between the concept of Chaser-Target and Follower-Leader. The first one is a functional classification, the second is a time arriving one. As Chaser the best choice is SAT1 because it is lighter, with higher acceleration and so it is more agile. It can change its strategy to gain the final arc easily orbit of the Target SAT2. The results are shown in Table 5.3

In Table 5.3 the difference between the strategy with SAT1 ahead or SAT2 ahead with 1N thrust is also shown. The difference is negligible from the results point of view, but from the theoretical point of view it is interesting to note that one solution is better than the other because follows the "'natural"' order of the unconstrained solution. It can be noted that the phasing constraint requires only 30g of propellant overall between the two satellites, so it is not a big deal with this type of spacecraft and thrust to mass ratio.

In the cooperative strategy both satellites are engaged to reach an optimum for the system and not only for the single satellite. This happens splitting the ΔV in such way that at the first apogee SAT1 has a lower energy than SAT2 (at least in the simplified model with only J2), so SAT2 becomes slower and permits with SAT1 to recover more easily the delay. This kind of approach saves only 10 g respect to the chaser-Target approach with 1N thrust, but it is one third of the fuel spent by the chaser target strategy. With more massive spacecraft or lower acceleration the benefit of cooperative approach will increase.

When luni-solar perturbations are involved the situation is more complex. The split between the phases are not more equal and so the two satellites can have different optimal structure in order to have Moon in favorable position (Fig. 5.18, 5.19), with arc vanishing also for fulfilling the final distance constraint. A one-year launch window starting December 1, 2015 has been analyzed, with 8 N thrust; the best performance (cooperative deployment) occurs for departure on January 21, 2016 and total final mass of 1959.9 kg (SAT1 851.5 kg, SAT2 1108.4 kg); almost equal performance is found for departure on July 31, 2016. The improvement, which can be obtained by so choosing the departure date that lunisolar perturbation is fully exploited, is therefore about 13 kg, with respect to the J2 model solution (total final mass of 1946.7 kg with nominal 8 N thrust). The final mass difference between the best departure date and the worst one is about 20kg.

5.3 Collision Avoidance

The satellite orbits are always very close, and the inter-satellite distance mainly depends on the delay which either satellite has with respect to the other. Since the orbital velocity is smaller at apogee, the minimum separation is expected to occur during the last apogee burn (when the orbits become very close). In fact, this anticipation holds for all the cases that have been treated in this work.

The satellite distance changes during the last burn, depending mainly on initial velocity, which may be different as the satellite orbits are not yet the same at the start of the propelled arc; thrusting has also an effect, as the engines are switched on and off at different times and the thrust accelerations are different. Perturbations

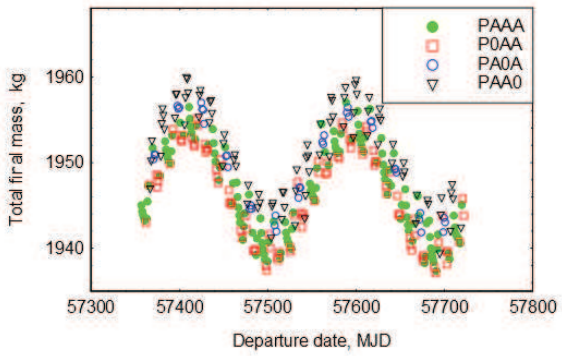

Figure 5.18: Switching function SAT1. Total final mass with departure date along 2016

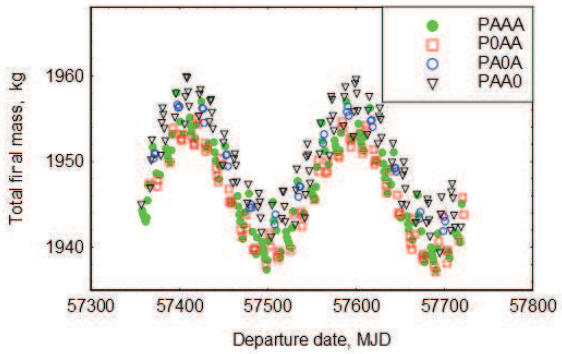

Figure 5.19: Switching function SAT2. Total final mass with departure date along 2016

have an additional influence, even through a very complex mechanism. The last revolution is not propelled, and therefore the satellite time-delay at the end of the last burn is almost equal to the final value; in the J2 model the inter-satellite distance is slightly greater than the nominal value for the formation, being velocity there greater than at final apogee, as the satellites are already moving towards the Earth. The last ballistic revolution undergoes other perturbations when the complete dynamic model is used: the radius of the second last apogee (and the corresponding velocity) differs from the final value and, in some cases, the inter-satellite distance after the last burn is a few hundred meters lower than the final separation (10 km). However, the satellite distance may be much smaller during the last burn, causing collision risks.

An exhaustive numerical analysis concerning the satellite separation during the

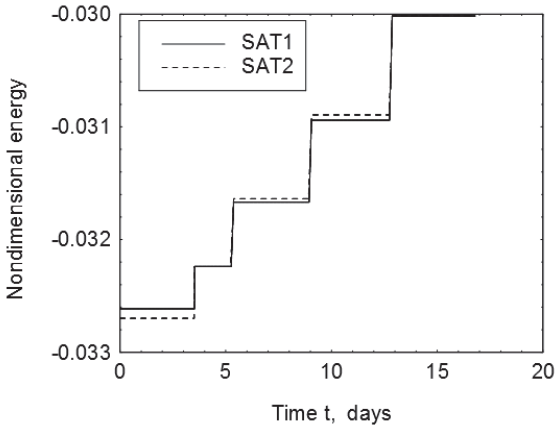

Figure 5.20: Energy of SAT1 and SAT2 with J2 perturbations only

maneuver has been carried out; cooperative deployment was only considered, and the J2 model was initially assumed. In this case SAT1 performs the first apogee burn to acquire a lower-energy lower-period orbit than SAT2, in order to recover the delay accumulated during the first revolution (see Figure 5.20). SAT2 cooperates using an opposite strategy, but at a minor extent, as the maneuver of the heavier satellite is less convenient. The satellites acquire the same energy only after the last burn. During this arc SAT2 has greater energy than SAT1 and is faster (the radius is the same and larger energy corresponds to higher velocity); therefore SAT2 follows SAT1 at the beginning of the last burn. This pattern is independent of the final configuration (SAT2 leading or trailing SAT1), as the gap recovered during the burn exceeds 10 km. Therefore, two different scenarios may occur. SAT2 overtakes SAT1 during the burn, when SAT2 is going to be the formation leader; minimum distance is typically about 6 km; the best performance is obtained in this case. On the other hand, if SAT1 will be eventually ahead in the deployed formation, two close approaches occur during the last burn. SAT2 initially overtakes SAT1 with a first passage at similar distance as in the former case, but SAT1 has larger thrust acceleration and eventually overtakes SAT2 with a very close approach (typically below 1 km) just before the burn end, when the spacecraft orbits are almost the same. In this case it is extremely difficult to constrain the inter-satellite minimum distance to a remarkably larger value.

The presence of perturbations does not change this picture significantly, even though Moon's gravity has a major effect on performance. Apogee burns are lengthened or shortened and the times of passage at apogees are adjusted to have the Moon in more favorable relative positions. Shorter initial burns and longer final burns reduce the mission length (energy is kept lower to reduce the orbital period); the

opposite strategy is adopted when a longer mission is useful. This kind of strategies is pursued at a greater extent by SAT1, which has larger acceleration and is less penalized by uneven split of the velocity gain among the apogee burns. However, it has been found that ,the energy of SAT2 is always larger before the last burn. The satellite relative position at the start of the last burn (i.e., SAT2 behind SAT1) is not changed by the account of perturbations; nevertheless, the previous scenario and the sequence of close approaches may be modified, depending on the energy difference between satellites.

The final thrust arcs of the most performing opportunities in terms of final mass are quite long, and the energy difference between satellites is still large before the last burn: the same conclusions as in the absence of perturbations hold. SAT2 overtakes SAT1 during the initial part of the burn, but the spacecraft separation remains quite large (typically above 5 km). This is the only close encounter, if SAT2 is going to be the formation leader. In the other case SAT1 must move ahead, causing a second short-distance (about 1 km) encounter. In these circumstances, the configuration with SAT2 ahead at the final point should be preferred. Inter-satellite distance and relative angular position for the mission departing on December 10, 2015 are shown in Figure 5.21, where apogees and perigees are highlighted by A and P, respectively (the first apogee burn vanishes in this mission); an enlargement of the last burn is presented in Figure 5.22.

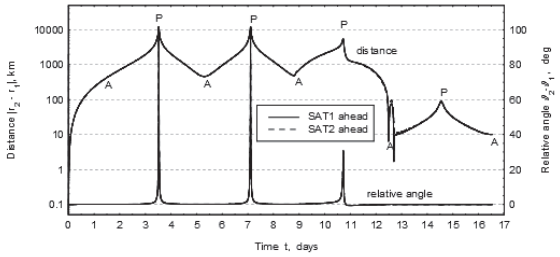

Figure 5.21: Inter-satellite distance 10 December 2015

The last burn is instead short in other cases, e.g., departing on December 2, 2015, and the energy difference between the spacecraft is small before the final thrust arc. These solutions are less interesting as they correspond to low-performance deployments. Satellite distance and relative angles are shown in Figures 5.23 and 5.25. In Figure 5.24 the switching point are shown. A very close approach (about 1 km) occurs, if SAT2 must be ahead at the final time, as SAT2 overtakes SAT1 when the satellites are moving on almost equal orbits. On the other hand, when SAT1 is selected as leader of the deployed formation, it remains ahead of SAT2 during the last burn and the minimum distance is usually only slightly lower than 10 km; this solution should be preferred to avoid collision risks.

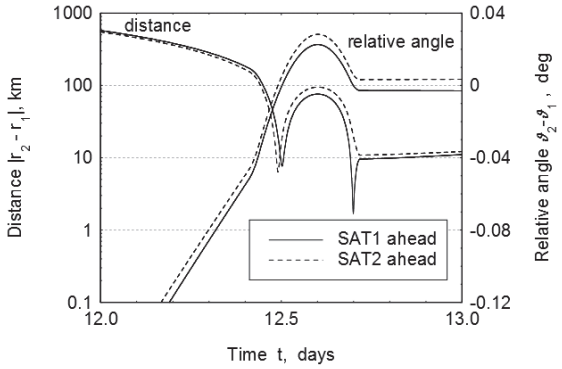

Figure 5.22: Inter-satellite distance 10 December 2015, magnification

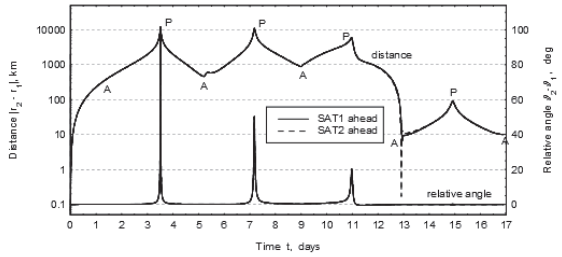

Figure 5.23: Inter-satellite distance 2 December 2015

The enforcement of a safety separation is useful to mitigate collision risks, but it is almost impossible to impose a large separation when a very close approach (e.g., 1 km) occurs during the unconstrained deployment, as in these cases the satellite minimum distance is attained close to the burn end, when the orbits are practically

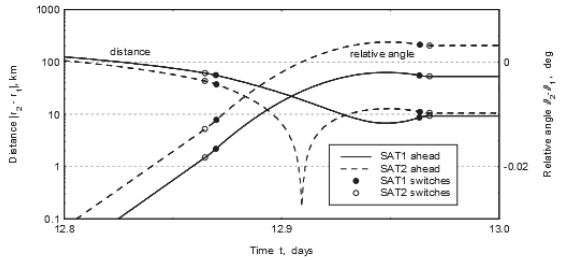

Figure 5.24: Inter-satellite distance 2 December 2015, magnification with switching points

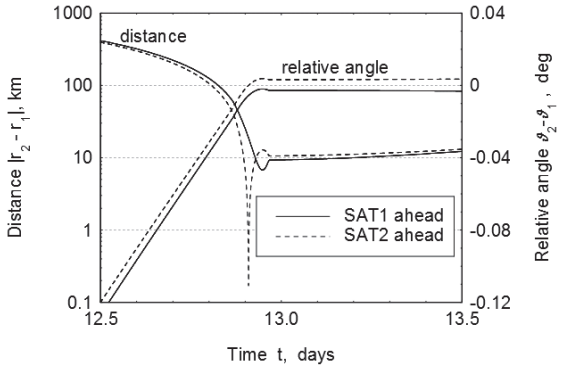

Figure 5.25: Inter-satellite distance 2 December 2015, magnification

equal. However, on the basis of the previous discussion, the formation leader can be chosen for any departure date so that the minimum distance of the unconstrained case is greater than 5 km. In this situation, separation can be easily increased by introducing the collision avoidance constraint described in Section 4.5.

An upper bound exists for the enforced separation and is close to the design value for the formation (i.e., 10 km), which in practice is already achieved at the end of the last burn; the actual limit value depends on the perturbations acting during the last ballistic revolution. The code typically converges to the optimal constrained solution in a few iterations, when the unconstrained solution is used as tentative guess and small values are assumed for the additional unknowns (i.e., $\Delta\lambda$).

Several tests have been carried out to evaluate how the introduction of a safety separation requirement affects performance. Tests have shown that the minimum distance can be increased from about 6 km to about 10 km with a negligible penalty on propellant consumption (less than 0.1 g). Also, no relevant differences are found in comparison to the simplified approach, which enforces a prescribed difference between the apogee radii of the satellites during the last burn. This approach should therefore be preferred as simpler and with a reduced number of unknowns to permit an easier and faster convergence. Almost equal results are found by the simplified approach, which enforces a prescribed difference between the apogee radii of the satellites during the last burn.

5.4 Optimal Constant-Direction Thrust

The optimal free direction thrust solution has β angle almost constant along each arc, while the α angle can vary between -10 and 10 degree, as Fig. 5.13 shows. If no thrust vectoring is present, changing thrust angles requires continuous attitude

Table 5.4: Final mass comparison with different control laws for SAT0 deployment.

	Dec. 25, 2012			Dec. 2, 2012		
Revs.	Optimal	α, β fixed	α, β optimal	Optimal	α, β fixed	α, β optimal
2.5	849.216	849.162	849.180	843.519	843.471	843.480
		-0.054	-0.036		-0.048	-0.039
3.5	848.982	848.941	848.970	843.784	843.752	843.770
		-0.041	-0.012		-0.032	-0.014
4.5	849.730	849.668	849.711	844.512	844.476	844.502
		-0.062	-0.019		-0.036	-0.010
5.5	851.153	851.084	851.137	843.663	843.564	843.614
		-0.069	-0.0167		-0.099	-0.049
6.5	851.014	850.920	850.997	844.188	844.092	844.178
		-0.094	-0.017		-0.096	-0.010

maneuvers in order to keep the thrust direction along the nominal one. Even if thrust vectoring is present, the thrust vector angles with respect to the body axes are constrained in amplitude and in changing ratio. Moreover, performing attitude maneuvers when the engine is on can increase thrust dispersion with respect to the nominal thrust profile.

Constant-direction thrust is a simpler control law. The angles value can be pre-assigned and so the optimization procedure finds only the time length of the burn arcs. However, this control law is too simple and it can not reach a final orbit with an assigned inclination.

Another option is to optimize the thrust angles of each burn arc. These angles are kept fixed along the single arc, but they can change from one arc to another.

The deployment of a single satellite (SAT0) is considered with increasing number of revolutions. As an example, performance for departure on December 25, 2015 (the most favorable case in December 2015) and December 2, 2015 are compared in Table 5.4. As expected, the resulting performance index is higher when optimal thrust angles, shown in Tables 5.5 (December 2) and 5.6 (December 25), are used in comparison to the simplified case with pre-assigned values; differences are however always very small. The benefit grows with the number of revolutions, i.e., apogee passages. It can be noted that the average value of β departs more remarkably from i_0 (5.2 degrees) when the number of apogee passages is increased; in this case, orbit plane change to encounter the Moon in more favorable configurations becomes more convenient.

Table 5.5: Optimal thrust angles for departure on December 2, 2015.

Revs.	P		A1		A2		A3		A4		A5	
	α	β	α	β	α	β	α	β	α	β	α	β
2.5	-0.1	-5.4	180.4	6.0	-	-	-	-	-	-	-	
3.5	-0.4	-5.5	180.6	6.4	180.5	6.4	-	-	-	-	-	-
4.5	-0.4	-5.5	180.6	6.7	180.6	6.7	180.4	6.7	-	-	-	-
5.5	-0.3	-5.5	-	-	-	-	180.7	7.3	180.7	7.3	-	-
6.5	-0.6	-5.5	180.8	7.9	-	-	-	-	180.8	8.0	181.1	8.0

Table 5.6: Optimal thrust angles for departure on December 25, 2015.

Revs.	P		A1		A2		A3		A4		A5	
	α	β	α	β	α	β	α	β	α	β	α	β
2.5	0.5	-6.2	180.3	6.5	-	-	-	-	-	-	-	-
3.5	0.4	-6.2	180.4	6.9	180.5	6.9	-	-	-	-	-	-
4.5	0.1	-6.2	180.5	7.2	180.7	7.2	-	-	-	-	-	-
5.5	0.1	-6.2	180.6	7.5	180.7	7.5	-	-	-	-	-	-
6.5	0.2	-6.2	-	-	-	-	-	-	180.8	7.9	180.8	7.9

5.5 Errors in control law

When the optimal constant-direction thrust law is chosen, dispersion is introduced to simulate an open loop mission. Errors can arise both in direction and thrust magnitude and are modeled as a random-bias Gaussian, fixed during each arc, plus white noise. A code that propagates solutions obtained from optimization (nominal control law) has been developed to simulate a mission without feedback and control. The output is the distribution of final perigee and apogee errors.

The 4.5-revolution mission with departure on December 2, 2015, which exhibits a PAAA optimal structure, is considered as an example. A test of a 100-run simulation with only thrust-direction dispersion was first performed ($3\sigma = 2.5$ deg); the final perigee error ranged between was -4 and $+2$ km, while final apogee error ranged from -6 to $+5$ km. Another 100-run simulation with also thrust magnitude errors ($3\sigma = 3\%T$) gave (quite obviously) much larger differences, namley between -139 and $+164$ km (perigee), and from -41 to $+36$ km (apogee). A similar behavior is found for any departure date; for instance, departure on December 25, 2015 (best solution in December, with PAA0 structure) has ranges between -136 and $+168$ km (perigee), and -44 and $+39$ km (apogee). Thrust dispersion affects the perigee height more remarkably, because it is achieved with long apogee burns and is therefore subject to large errors; on the contrary, errors on apogee height are

smaller, as they are generated by thrust dispersion during a short perigee burn and, only to a minor extent, during apogee burns (see Fig. 5.26,5.27,5.28,5.29,5.30).

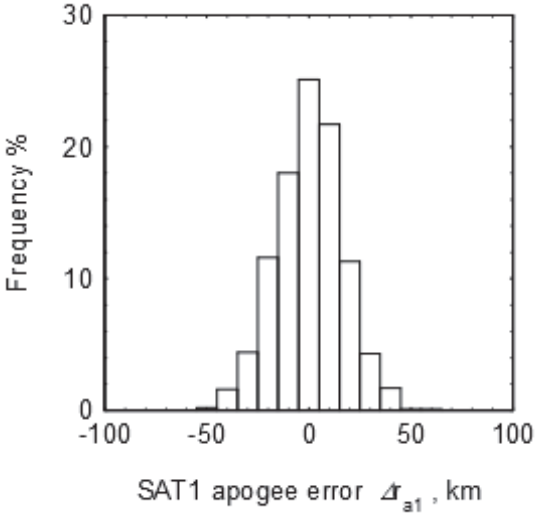

Figure 5.26: r_a SAT1 dispersion

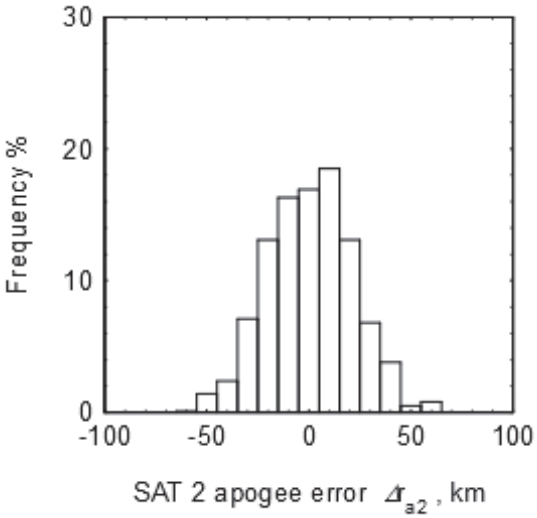

Figure 5.27: r_a SAT2 dispersion

A procedure was developed to simulate missions with feedback control, as shown in 5.31. After each apogee burn the state of the spacecraft is used as a new starting

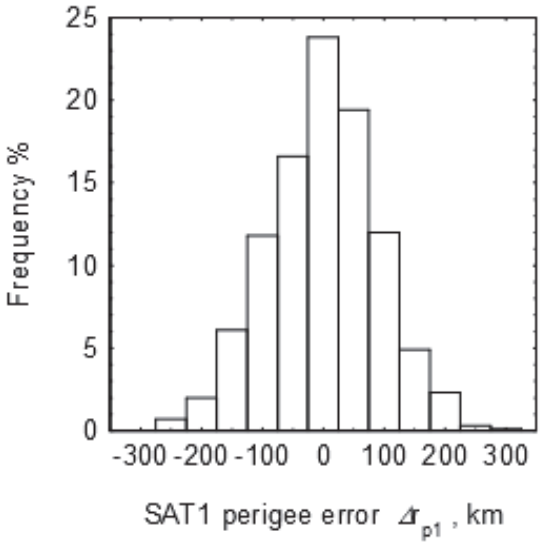

Figure 5.28: r_p SAT1 dispersion

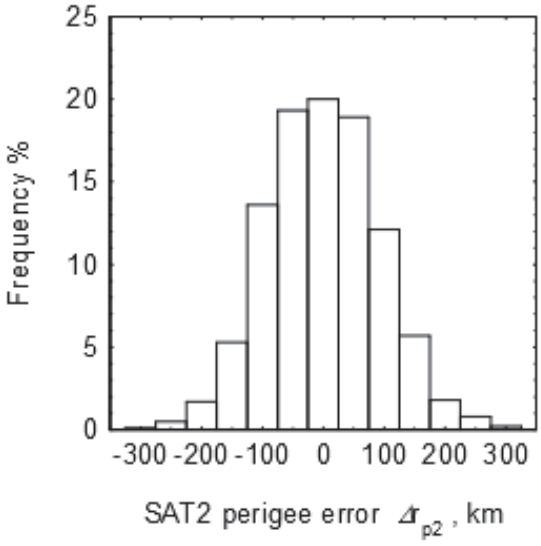

Figure 5.29: r_p SAT2 dispersion

point and the optimal deployment with constant-direction thrust is re-evaluated, while preserving the total number of revolutions. The starting point, in this case,

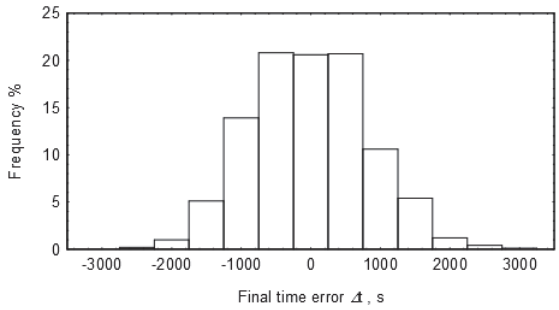

Figure 5.30: Final phasing time dispersion

are the observation points O_1 and O_2 (look at Fig. 5.32). The procedure of re-optimization was done manually with the purpose of simulating a correction after the satellite tracking, as in a MPC controller. The new initial state is considered acquired without error. One should note that sometimes the optimal burn structure in the presence of dispersions can be different from that of the nominal case: for example, an additional perigee burn may be required or an apogee arc may vanish or appear, depending on the actual thrust history during the previous burns. Not all possible cases have been analyzed here, but the original burn structure was maintained, even though not optimal; test cases have shown that the final mass penalty is always very small. The only modification was the addition of an apogee burn at the last apogee passage before orbit insertion for those trajectories which did not have it, as this burn is mandatory for the correction of errors accumulated during previous burns.

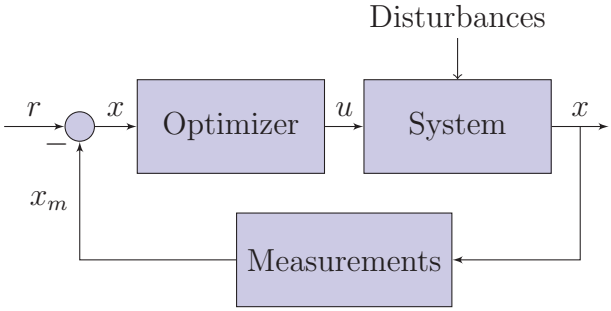

Figure 5.31: Re-optimization Scheme

The procedure is here described for a 4.5-revolution mission. The trajectory is optimized without thrusting dispersion and the nominal optimal control law (switching times and thrust angles α_j and β_j during each burn) is obtained. The nominal

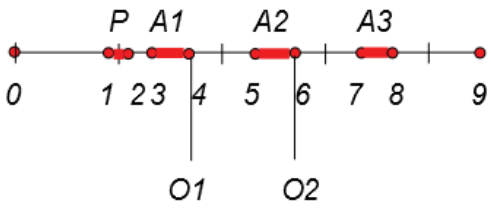

Figure 5.32: Observation points in mission timeline

control law is then adopted during the perigee (P) and first apogee (A1) burns and the spacecraft state after A1 in the presence of thrust dispersion is evaluated. A new mission starting with this state is optimized without thrusting dispersion and the updated control law for the following apogee burns (i.e., A2 and A3) is obtained. Dispersions are again introduced during the second burn and the state at its end is obtained. A new optimization is finally carried out with this departure state to obtained an updated law for A3, and thrust dispersion is then introduced during A3 to evaluate final perigee and apogee errors.

It is important to note that when the last arc is shorter, final errors with the updated control law are smaller (apogee and perigee differ from the prescribed values by less than 1 km). On the contrary, when the updated optimal trajectory requires a long last burn, the final error remains unacceptable (tens of kilometers) when dispersion during this arc is considered, even after re-optimization. The relevant point is that the final error is the result of all thrust errors occurred during maneuvers. Errors during the perigee and the first two apogee maneuvers can be compensated by tracking the satellite state and re-designing the final burn of the trajectory. In the absence of thrust dispersion during the final burn, the required final state would be achieved exactly; however, the errors arising during the last maneuver cannot be compensated. Since these errors are related to the burn length, small final errors are experienced when the last burn has a low ΔV.

For this reason, final orbit errors (after the control law has been updated) are smaller when the nominal mission has a PAA0 structure; in fact, during the last apogee passage (A3), a short burn is introduced only to correct the errors accumulated during P, A1 and A2; errors during this burn only slightly affect the final orbit, due to the short duration. It is important to remark that PAA0 is the optimal structure of the best performing missions, and better error compensation adds a further benefit. As an example, two missions with different structure (PAAA, departure December 2, and PAA0, departure December 25) and similar final errors (before control law update) are compared. In particular, two simulations in the presence of

dispersion are chosen, so as both missions show similar perigee and apogee errors, namely, about +100 km and −15 km, respectively. The perigee error is larger, due to the longer apogee burns required for perigee raising.

After the correction procedure is applied, the mission with departure on December 25 exhibits almost null errors (+39 m and +196 m for perigee and apogee, respectively): a very short (30 s) A3 burn is required to correct errors arising during the former maneuvers (note that errors caused during P and A1 are also partially compensated during the re-optimized A2) and errors are therefore only marginal. On the other hand, A3 burn is 1 hour 53 minutes long in the nominal case when the departure date is December 2, and becomes 2 hours 28 minutes when the control law is updated to correct the errors caused by previous burns (in the first re-optimization A2 length is reduced, causing an increase of A3 length); the effects of dispersion during this long burn are much larger, and final errors are about +10 km on perigee and −250 m on apogee. These considerations suggest that a PAA0 nominal trajectory should always be adopted, notwithstanding the optimal structure being different on the particular departure date which is considered (the penalty is always less than 300 g, with larger values corresponding to the worst missions with P0AA optimal structure). Final masses of PAA0 solutions and optimal solutions are compared in Fig. 5.33 for 4.5-revolution missions with departure in December 2015. Full and empty triangles denote PAA0 solutions when they are optimal and non-optimal, respectively. Once dispersions during P and A1 are introduced, an updated control law is evaluated and adopted for A2 (no thrust is considered during A3, at this point). After dispersions during A2 are introduced, the final burn A3 is finally added and optimized; its short duration is required only to accommodate errors which arose during A2. Errors less than 1 km for both apogee and perigee have always been obtained for many test cases considered. In the previous example with departure on December 2, errors with the updated control law become −84 m (perigee) and +4 m (apogee) as the final burn is now only about 1 minute 37 seconds long. The mass penalty is only 15 grams compared to the optimal PAA0 solution, but the final orbit is now achieved with a much larger accuracy.

Convergence may be difficult when the final A3 burn is introduced to correct the errors for a PAA0 trajectory; this issue arises when dispersion during the first burn is such that the final perigee height is larger than the prescribed value and a perigee lowering is required; when the nominal solution is used as tentative value thrust and primer vectors have opposite direction and the switching function is always negative, preventing convergence. This problem can be solved by imposing an A3 burn with very short duration (8 s has been used here) in the starting nominal structure. This short burn does not substantially modify the lengths of the other arcs and the capability of the control procedure to compensate for thrusting dispersion and achieve the final orbit with great accuracy; however, the forced presence of a thrusting A3 arc during the previous phases of the control procedure, causes the

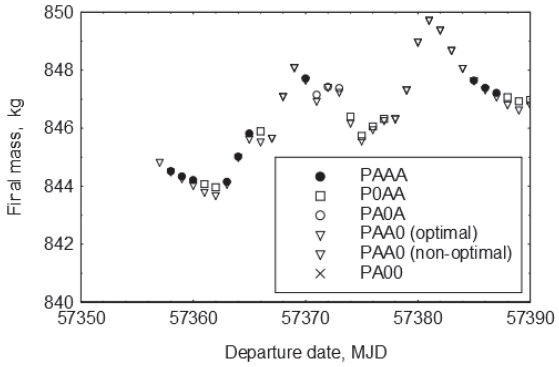

Figure 5.33: Comparison between PAAA and PAA0 solutions

solutions to have always a final perigee raising even when dispersion is introduced, thus permitting an easier convergence.

Conclusions

The results of single satellite deployment shows that high thrust and multi-revolution increases final mass. The influence of Earth oblateness, due mainly to J2, changes the thrust strategy from A-A-..-P to P-A-A-... The effects od Moon and Sun perbations on the optimal solution are more complex. They can increase or decrease the final satellite mass, depending on the Moon and Sun angular position w.r.t. satellite when it is at the apogee. In order to find the perturbing body, mainly the Moon, in the favorable position the optimal thrust strategy changes time thrust length, depending on the launch date. Solar Radiation Pressure has not shown any remarkble influence in the satellite performance index and strategy. The thrust strategy changes also when the formation flight is considered and the final distance boundary constraint is introduced. The cooperative deployment has shown to be better then chaser target one, but the difference is small for this type of mission and satellite.

Collision avoidance is also analyzed. Even if it is possible to constraint the minimum inter-satellite distance, the best strategy is to choice which satellite arrives first at the last apogee, depending on the last thrust arc length.

The final section shows the effects of thrust dispersion errors on the final reached orbit, that is different from the prescribed one. The re-optimization procedure shown to be effective in recovering the error with a small penalty if the final thrust arc is kept small.

Conclusions

The work done in these three years and exposed in the thesis shows a large number of interesting results. Deployment missions with high interest but scarcely considered in literature have been analyzed. Starting from the case study of Simbol-X, the indirect optimization method developed at Politecnico di Torino was improved. The results of this thesis can be divided in two parts: the results concerning the case study mission and the improvements of the method.

The indirect optimization method is concerned, subroutines for handling asphericity of the Earth perturbations, third bodies perturbations and solar radiation pressure have been developed. Also constraints for formation flight with different phasing strategies have been derived, opening to new interesting problems. Convergence is easily achieved thanks to a peculiar continuation technique developed in this thesis. A first tentative of robust optimization has been developed.

The new tool can be used for studying many Earth-centered missions, but can be easily adapted also for Jupiter-centered mission, such as mission towards Europe and other Galilean Moons. The influence of third-body perturbations could be useful also for interplanetary trajectories, i.e. Jupiter perturbations in Earth-Mars transfer. The optimization procedure is able to find trajectories where third bodies are in favorable position, maybe suggesting in some case flyby opportunities.

The cooperative strategy, united with collision avoidance analysis, can be useful for studying the deployment of others formation flight or swarm mission. Also the deployment in orbit of big auto-assembling modules for Deep Space Habitat can be studied.

From the point of view of the mission, the launch window was widely analyzed, with different times of flight and different thrust levels. A reliable procedure for finding the optimal solution was developed and tested. The procedure permits to choose a proper departure date, avoiding the plumbing of the two satellites into the atmosphere. The effects of perturbations on the transfer have been studied in details, highlighting how Moon and Sun strongly influence trajectory performance and optimal control strategy. The final mass exhibits changes up to 40 kg depending on the departure date. An approximate control law, which is more easy to use in a real mission because involves fewer attitude maneuvers than the optimal law

was also considered. For the formation flight it was found that the cooperative strategy improves the formation final mass, but the difference from the chaser target strategy is not significant, at least when the thrust is sufficiently large. So for a first design analysis the chaser target strategy can represent a cheaper analysis from the computational point of view.

During formation deployment the inter-satellite distance can be small and increasing collision risk. In order to avoid this issue, a minimum distance constraint has been introduced. The collision avoidance analysis showed that not all possible configurations (leader-follower) can fulfill this constraint, so the best thing is to adopt the right configuration strategy. Considering that the thrust strategy depends on luni-solar perturbation, choosing which satellites arrives first at the apogee is fundamental. The more favorable configuration is not equal for all the departure dates, but understanding which variables influence the minimal distance, gives an insight to find the right configuration.

The problem of thrust dispersion errors was also analyzed. A brief sensitivity analysis was carried out using some not-nominal thrust profile scenarios. The optimization procedure has been applied in a closed loop. The optimal nominal solution showed to be not enough robust when dealing with recovering errors. When satellites are tracked in a finite number of points during the transfer, the best heuristic strategy found is to have a short last burn arc. The last burn can produce only few errors and the final point is reached with a very good accuracy. This can be a good starting point for future works aiming at robust optimization.

Appendix A

Ringraziamenti finali e Aknowledgements

Per chi ha avuto la forza di arrivare al termine di questo lavoro, una paio di pagine omaggio in cui voglio ringraziare le persone che mi hanno accompagnato in questi tre anni di dottorato al Politecnico di Torino. Poiché, nonostante la mia proverbiale pigrizia e inerzia, sono stato un po' internazionale, questi ringraziamenti passeranno dall'italiano all'inglese senza un grande filo logico. Inoltre, come potrete notare, il mio già traballante italiano, ormai èin caduta libera grazie al mio terrificante inglese.

Innanzitutto ringrazio il CNES. Il lavoro presentato in questa tesi di dottorato è stato possibile grazie all'assegno di ricerca del Politecnico di Torino, finanziato dal Centre National d'Etudes Spatiales (CNES), [Numero di Contratto 93333/00]. A supervisionare il progetto durante tutte le sue fasi è stato l'ingegnere Richard Epenoy, che ringrazio sia per la disponibilità che per la cordialità, anche successivamente la fine del contratto.

Senza pero' la guida, l'esperienza ed il lavoro del professor Casalino non avrei potuto ottenere questi risultati. Ringrazio quindi il professor Lorenzo Casalino, che, come relatore e professore, mi segue fin dalla laurea triennale. In questi anni ho avuto modo di imparare molto da lui. Lo ringrazio per essere stato la mia guida paziente in questi anni. Spero nel futuro di poter accrescere le mie capacità e competenze per poi trasmetterle ad altri "ottimizzatori".

Ringrazio il prof. Guido Colasurdo e Alessandro Zavoli, con i quali abbiamo collaborato per il progetto sul dispiegamento dei satelliti in HEO e con cui condivido gran parte del lavoro esposto in questa tesi. Per me è stato molto importante avere la possibilità di discutere e condividere le mie idee, anche le più stupide, con un dottorando come me.

Ringrazio il prof. Dario Pastrone con cui ho potuto collaborare, in particolar modo sull'ottimizzazione di motori ibridi. Ma non posso che ringraziare lui, insieme sempre al prof. Casalino, per la compagnia in tre anni di pranzi al Politecnico. Mi

spiace solo che le mie qualità enologiche non abbiano dato abbastanza soddisfazione nei pranzi da Ostu.

Ringrazio Francesca Letizia che, anche se per un breve periodo, ha condiviso l'ufficio con me, dandomi la possibilita' di interessanti e vivaci discussioni che andavano dall'astrodinamica, all'antropologia ed alla politica. E anche al vestiario...

Ringrazio anche tutti coloro che, nel passato, hanno contribuito a creare e modificare i programmi con i quali ho lavorato. Sicuramente partendo dal professor Bussi, per poi passare dal prof Colasurdo, Casalino, Pastrone e a Matteo Rosa Sentinella più altri che non ho mai conscoiuto. In questi anni ho avuto anche l'opportunità di partecipare a 3 GTOC (Global Trajectory Optimization Competition)e ringrazio tutti coloro che le hanno organizzate, ma sicuramente un grosso grazie alle persone che hanno lavorato con me. Nella GTOC6 il gruppo del Politecnico di Torino e Università Sapienza di Roma è riuscito ad arrivare primo. Ringrazio quindi Alessandro Longo e Stefano Federici che, insieme ai già citati Casalino, Colasurdo, Alessandro Z e Francesca sono riusciti a conquistare il primo premio con un mio piccolo contributo dall'estero. Ringrazio inoltre Matteo per avermi dato suggerimenti per le mie prime lezioni dall'altra parte della cattedra.

I thank also HongXin Shen, my office mate in the last period in Politecnico. Thank you for the optimization and Moon travel discussions. I hope to see you again in the future.

During my last 6 months of PhD I had the opportunity to study at JPL in Pasadena. This period abroad was possible thanks to the JPL-Polito agreement, the work of Cinzia Zuffada, Chief Scientist assistent at JPL, and JPL and Caltech staff (we don't forget Albert Magallanes). From Polito side Fabrizio Pirri was the organizer. The experience was possible thanks to BAF (Bando Alta Formazione) fundings. In the JPL summer Nathan Strange was my mentor and I want to thank him for his advices and his welcoming. He was a fixed point inside and outside the Lab (as Nitin said, he was our Sun and we were all in the two body problem). I hope I will finish my cycler paper, soon or later!

And then we were us, the Fantasti 4, the 4 Nathan's student: Nitin, Farah, Jules and me. They help me since the first day and It was a wonderful time to stay with them. And I like to think that Jimyn is my far nephew :D

They were not the only one that makes my JPL summer unforgiveble: there are also Raul, Claire and Hui-Ying. Obviously a special thanks is for Raul that was my European office mate, my donuts pusher. How many talks we made on the white-board about space and satellite? And how can forget that we chase a Space Shuttle in L.A. streets in the middle of the night?

I want to thank also all the astrodynamic group, that was always source of inspiration and fun: Stass, Stafano, Damon, Gregory, Greg, Daniel, Demyan, Jeff and I hope I am not forgettig anyone.

Ovviamente non posso dimetnicare i miei compagni di viaggio che son partiti con

me da Torino, affrontando la maledizione delle mille mail: Luca, Alberto, Antonio, Alessandro ed Eleonora. Ci aggiungo anche roberto, che essendo aerospaziale, è come se fosse partito con noi.

Chiaramente per Eleonora è un capitolo un po' a parte. Seguiamo lo stesso percorso da ormai tanto tempo: abbiamo portato avanti la fiaccola per 5 anni di ingegneria aerospaziale, poi per un anno di stage, poi per tre anni di dottorato e anche negli States! Bè, mi sa che a Pasadena è stata la fiaccola a portare noi... Se la vita fosse un film direi: "É stato un onore combattere al suo fianco".

Per concludere il capitolo americano, un immenso ringraziamento va a Maddalena e Riccardo, che mi hanno trattato come un figlio, facendomi sentire a casa mia anche se ero dall'altra parte del globo. Ringrazio anche la loro famiglia (Gilberto in particolar modo) e tutto il vicinato di Casa Grande Street.

Ritornando in Italia, ringrazio invece gli altri dottorandi che hanno affrontato con me questo percorso e mi hanno accolto (anche se sopportato sarebbe il termine più adeguato) nei momenti di solitudine pomeridiana: Federico, i due Alberti, Davide, Alessandra, Elena, Matteo e Marianna.

E poi... e poi... e poi sarà come morire... E poi ci sono gli amici, sparsi per l'Italia, l'Europa e i continenti neanche fossero le sfere del drago. Li ringrazio tutti per le serate, le chiaccherate, i consigli e il tempo, quale preziosa risorsa, passato insieme: Nathalie, Paolo, Federico, Edo, Mattia, Gabriele, Claudia, Francesco, Sara, Giuseppe, Pierfrancesco, Pierangelo, Stefania, Matteo, Michele. Un poco ringrazio anche Vera, ma non troppo.

Per la fiducia invece non ringrazio nessuno.

E siamo arrivati alla fine? No, direi di no. Manca ancora l'ultimo tassello. La famiglia. Che non è un nome collettivo astratto, ma un insieme concreto di persone che mi son sempre vicine: i miei zii e miei cugini. Che sono tanti. E poi ci sono i figli dei cugini. E tra un poco forse anche loro avranno dei figli. Che tutti pensano che mi inventi le cose come Aldo nella canzone di Elio e le Storie Tese quando dico "Mio cugino ha fatto questo". E invece è solo che sono tanti. Ed è bello così.

Arriviamo quindi alla cerchia più stretta, tipo il cerchio della morte e della vita. Ringrazio mio padre, che mi sta vicino come può.

Ringrazio poi mia sorella, ma non sempre, a tratti. Qualche volta. Poche volte. É che alcune volte (tutte le altre) è difficile vivere con se stessi, figuriamoci con gli altri.

E poi ringrazio mia madre, che son dieci anni che sono andato via per la mia strada e spero che ogni tanto sia fiera di me.

E quindi uscimmo a riveder le stelle. Ma solo se non piove.

Bibliography

[1] J. Fontdecaba , G. Métris , P. Gamet , P. Exertier, "'Solar radiation pressure effects on very high-eccentric formation flying"',Proceedings of the 3rd International Symposium on Formation Flying, Missions and Technologies, 23-25/04/2008,Noordwijk,Pays-Bas

[2] E. Wnuk, Accuracy of predicted earth's artificial satellite orbits, Advances in Space Research, Volume 16, Issue 12, 1995, Pages 101-104, ISSN 0273-1177, 10.1016/0273-1177(95)98790-U. (http://www.sciencedirect.com/science/article/pii/027311779598790U)

[3] Edwin Wnuk, Recent progress in analytical orbit theories, Advances in Space Research, Volume 23, Issue 4, 1999, Pages 677-687, ISSN 0273-1177, 10.1016/S0273-1177(99)00148-9. (http://www.sciencedirect.com/science/article/pii/S0273117799001489)

[4] Siebold, K. H. and Reynolds, R., C., "'Lifetime Reduction of a Geosynchronous Transfer Orbit with the Help of Lunar-Solar Perturbations"', Advances in Space Research, vol. 16, No. 11, (11)155-(11)161, 1995

[5] Martynenko, B. K.,Lunar-solar gravitational perturbations for artificial satellite with twenty-four hour sidereal, Marshall Space Flight Center, 1967

[6] Fisher, D.,"'Lunisolar perturbations of the motion of artificial satellites"', Goddard Space Flight Center, NASA-TM-X-65476, X-552-71-60, 1971

[7] Fisher, D.,"'Analytic short period lunar and solar perturbations of artificial satellites"', Goddard Space Flight Center, NASA-TM-X-65869, X-552-72-83, 1972

[8] Kechichian, J.A., "Analytic Expansions of Luni-Solar Gravity Perturbations Along Rotating Axes for Trajectory Optimization: Part 1: The Dynamic System," *Acta Astronautica*, Vol. 68, No. 3, 2011, pp. 1947–1963. doi:10.1016/j.actaastro.2010.12.001.

[9] Kechichian, J.A., "Analytic Expansions of Luni-Solar Gravity Perturbations Along Rotating Axes for Trajectory Optimization: Part 2: The Multipliers System and Simulations," *Acta Astronautica*, Vol. 68, No. 3, 2011, pp. 1914–1930. doi:10.1016/j.actaastro.2010.12.003.

[10] Sims, Jon A.; Finlayson, Paul A.; Rinderle, Edward A.; Vavrina, Matthew A.;

Kowalkowski, Theresa D.,"'Implementation of a Low-Thrust Trajectory Optimization Algorithm for Preliminary Design"', Jet Propulsion Laboratory, 2006 Online Source: hdl:2014/40263

[11] Author: Whiffen, Gregory J., "'Mystic: Implementation of the Static Dynamic Optimal Control Algorithm for High-Fidelity, Low-Thrust Trajectory Design"',Jet Propulsion Laboratory, 2006 Online Source: hdl:2014/40782

[12] Geffroy, S., and Epenoy, R., "Optimal Low-Thrust Transfer with Constraints - Generalization of Averaging Techniques," *Acta Astronautica*, Vol. 41, No. 3, 1997, pp. 133-149. doi:10.1016/S0094-5765(97)00208-7.

[13] Redding, D.C., and Breakwell, J.V., "Optimal Low-Thrust Transfers to Synchronous Orbit," *Journal of Guidance, Control, and Dynamics*, Vol. 7, No. 2, 1984, pp. 148-155. doi: 10.2514/3.8560.

[14] Bertrand, R., and Epenoy, R., "New Smoothing Techniques for Solving Bang-bang Optimal Control Problems - Numerical Results and Statistical Interpretation," *Optimal Control Applications and Methods*, Vol. 23, 2002, pp. 171-197. doi 10.1002/oca.709.

[15] Haberkorn, T., and Martinon, P., "Low-Thrust Minimum-Fuel Orbital Transfer: A Homotopic Approach," *Journal of Guidance, Control, and Dynamics*, Vol. 27, No. 6, 2004, pp. 1046-1060. doi: 10.2514/1.4022.

[16] Thevenet, J.-B., and Epenoy, R., "Minimum-Fuel Deployment for Spacecraft Formations via Optimal Control," *Journal of Guidance, Control, and Dynamics*, Vol. 31, No. 1, 2008, pp. 101-113. doi: 10.2514/1.23181.

[17] Chuang, J.C.H., Goodson, T.D., and Hanson, J., "Multiple-Burn Families of Optimal Low- and Medium-Thrust Orbit Transfers," *Journal of Spacecraft and Rockets*, Vol. 36, No. 6, 1999, pp. 866-874. doi: 10.2514/2.3505.

[18] Colasurdo, G., and Casalino, L., "Missions to Asteroids Using Solar Electric Propulsion," *Acta Astronautica*, Vol. 50, No. 11, 2002, pp. 705-711. doi: 10.1016/S0094-5765(03)80012-7.

[19] Colasurdo, G., and Casalino, L., "Optimal Control Law for Interplanetary Trajectories with Nonideal Solar Sail," *Journal of Spacecraft and Rockets*, Vol. 40, No. 2, 2003, pp. 260-265. doi: 10.2514/2.3941.

[20] Casalino, L., and Colasurdo, G., "Optimization of Variable-Specific-Impulse Interplanetary Trajectories," *Journal of Guidance, Control, and Dynamics*, Vol. 27, No. 4, 2004, pp. 678-684. doi: 10.2514/1.11159.

[21] Casalino, L. Colasurdo, G. and Pastrone , D., "Optimal Low-Thrust Escape Trajectories Using Gravity Assist," *Journal of Guidance, Control, and Dynamics*, Vol. 22 No. 5, 1999, pp. 637–642. doi: 10.2514/2.4451.

[22] Casalino, L., Colasurdo, G., and Pastrone, D., "Optimization Procedure for Preliminary Design of Opposition-Class Mars Missions," *Journal of Guidance, Control, and Dynamics*, Vol. 21, No. 1, 1998, pp. 134-140. doi: 10.2514/2.4209.

[23] Casalino, L., Pastrone, D., Colasurdo, G., "Integrated Design of Hybrid Rocket Upper Stage and Launcher Trajectory," 45th AIAA/ASME/SAE/ASEE Joint Propulsion Conference and Exhibit, August, 2-5, 2009, Denver, Colorado. Paper AIAA 2009-4843.

[24] Casalino, L., "Singular Arc During Aerocruise," *Journal of Guidance, Control, and Dynamics*, Vol. 23, No. 1, 2000, pp. 118-123. doi: 10.2514/2.4494.

[25] La Mantia, M., and Casalino, L., "Indirect Optimization of Low-Thrust Capture Trajectories," *Journal of Guidance, Control, and Dynamics*, Vol. 29, No. 4, 2006, pp. 1011-1014. doi: 10.2514/1.18986.

[26] Gamet, P., Epenoy, R., and Salcedo, C., "SIMBOL-X: A Formation Flying Mission on HEO for Exploring the Universe," 20th ISSFD, Annapolis, MD, September 2007. NASA Technical Report Service, ID: 20080012679.

[27] Pascal, Gamet, "'Prelaunch analysis of the orbit determination for the Simbol-X mission"', 21st ISSFD 2009, September 28 - October 2, 2009, Toulouse

[28] http://143.225.92.211/cms/index.php?page=metodi-e-tecniche-di-ottimizzazione-innovative-per-applicazioni-elettromagnetiche

[29] EE364a: Convex Optimization Professor Stephen Boyd, Stanford University

[30] Stengel, Optimal Control and Estimation, MAE 546, Princeton http://www.princeton.edu/štengel/MAE546.html

[31] Betts, T., "Survey of Numerical Methods for Trajectory Optimization," *Journal of Guidance, Control, and Dynamics*, Vol. 21, No. 2, 1998, pp. 193–207. doi: 10.2514/2.4231.

[32] Petropoulos, Anastassios E., "'Refinements to the Q-law for the low-thrust orbit transfers"',Jan-2005, Pasadena, CA : Jet Propulsion Laboratory, National Aeronautics and Space Administration, 2005, 15th AAS/AIAA Space Flight Mechanics Conference, Copper Mountain, CO, January 23-27, 2005 URI: http://hdl.handle.net/2014/37521

[33] M. Rosa Sentinella, "'Comparison and Integrated Use of Differential Evolution and Genetic Algorithms for Space Trajectory Optimisation"',Proceedings of the 2007 IEEE Congress on Evolutionary Computation,2007,Singapore,973–978

[34] Rosa Sentinella, M. and Casalino, L. "'Hybrid evolutionary algorithm for the optimization of interplanetary trajectories"'. J. Spacecraft and Rockets, 2009, 46, 365-372.

[35] Rosa Sentinella, M. and Casalino, L. "'Cooperative evolutionary algorithm for space trajectory optimization."' Celestial Mech. Dyn. Astron. 2009, 105, 211-227

[36] J.H. Holland, "'Adaption in natural and artificial systems"', Ann Arbor: University of Michigan Press, 1975

[37] Deb, K. "'An introduction to genetic algorithms."' Sa¯dhana¯ J., 2009, 24, 293-315.

[38] Storn, R. 'On the usage of differential evolution for function optimization"', 1996 Biennial Conference of the North American Fuzzy Information Processing

Society, Berkeley, California, 19-22 June 1996, pp. 519-523 (IEEE, Piscataway, New Jersey).

[39] Storn, R. and Price, K. "'Differential evolution - a simple and efficient adaptive scheme for global optimization over continuous spaces."' TR-95-012

[40] J. Kennedy, and R.C. Eberhart, "Particle swarm optimisation", Proceedings of the IEEE International Conference on Neural Networks, pp. 1942-1948, 1995.

[41] R.C. Eberhart, and J. Kennedy, "A new optimizer using Particle swarm theory", Sixth International Synposium on Micro Machine and Human Science, pp. 39-43, 1995.

[42] J. Kennedy, "The PSO: social adaption of knowledge", Proceedings of the IEEE International Conference on Evolutionary Computation, Indianapolis, Indiana, pp. 303-310, 1997.

[43] M. Clerc, and J. Kennedy, "The Particle swarm explosion, stability, and convergence in a multidimensional complex space", IEEE Transaction on Evolutionary Computation, Vol. 6, pp. 58-73, 2002.

[44] Trelea, I. C. "'The particle swarm optimization algorithm: Convergence analysis and parameter selection."' Inform. Process. Lett., 2003, 85, 317-325.

[45] Colorni, M. Dorigo et V. Maniezzo, Distributed Optimization by Ant Colonies, actes de la première conférence européenne sur la vie artificielle, Paris, France, Elsevier Publishing, 134-142, 1991.

[46] M. Dorigo, Optimization, Learning and Natural Algorithms, PhD thesis, Politecnico di Milano, Italie, 1992

[47] A. H. Land and A. G. Doig (1960). "'An automatic method of solving discrete programming problems"'. Econometrica 28 (3): pp. 497-520. doi:10.2307/1910129

[48] Kirkpatrick, S.; Gelatt, C. D.; Vecchi, M. P. (1983). "'Optimization by simulated Annealing"'. Science 220 (4598): 671-680. doi:10.1126/science.220.4598.671. JSTOR 1690046

[49] Glover, F. "'Tabu search: Part i."' ORSA J. Comput. 1989, 1, 190-206.

[50] Glover, F. "'Tabu search: Part ii."' ORSA Journal on Computing., 1990, 2, 4-32.

[51] Chelouah, R. and Siarry, P. "'Tabu search applied to global optimization."' Eur. J. Operat. Res., 2000, 123, 256-270.

[52] Siarry, P. and Berthiau, G. "'Fitting of tabu search to optimize functions of continuous variables."' Int. J. Numer. Methods Eng., 1997, 40, 2449-2457.

[53] Bryson, A. E., and Ho, Y.-C., *Applied Optimal Control,* rev. ed., Hemisphere, Washington, DC, 1975, pp. 42–89.

[54] Moulton, F.R., *New Methods in Exterior Ballistics*, Univ. of Chicago, Chicago, IL, 1926.

[55] D.F. Shampine, M.K. Gordon, *Computer Solution of ordinary differential equation: the initial value problem*, W.H. Freeman, S. Francisco, 1975

[56] Roger R. Bate, Donald D. Mueller, Jerry E. White, "'Fundamentals of Astrodynamics"', Courier Dover Publications, 1971 - Science - 455 pages

[57] J. W. Cornelisse, H. F. R. Schöyer, K. F. Wakker., "'Rocket propulsion and spaceflight dynamics "' Published 1979 by Pitman in London, San Francisco

[58] Wagner, C. A., *The gravity potential and force field of the Earth through fourth order*, NASA-TN-D-3317, NASA Goddard Space Flight Center, 1966

[59] Anonymous, *World Geodetic System 1984, Its Definition and Relationships With Local Geodetic Systems*, NIMA Technical Report TR8350.2, Department of Defense, Third Edition, National Geospatial-Intelligence Agency, January 2000.

[60] Anonymous, EGM 2008 Model coefficients - Original Release, National Geospatial-Intelligence Agency. http://earth-info.nga.mil/GandG/wgs84/ gravitymod/egm2008/first_release.html [retrived October 27, 2011].

[61] Abramowitz, M. and Stegun, I. A. (Eds.), *Handbook of Mathematical Functions with Formulas, Graphs, and Mathematical Tables*, 9th printing, Dover, New York, 1972,"Legendre Functions", Ch.8, pp. 331-339 and "Orthogonal Polynomials", Ch. 22, pp. 771-802.

[62] Bosch, W., "On the Computation of Derivatives of Legendre Functions," *Physics and Chemistry of the Earth, Part A: Solid Earth and Geodesy*, Vol. 25, Issues 9-11, 2000, pp. 655-659.

[63] Russell, R. P., Arora, N., Global Point Mascon Models for Simple, Accurate and Parallel Geopotential Computation, Journal of Guidance, Control, and Dynamics, Vol. 35, No. 5, 2012, pp. 1568-1581, DOI: 10.2514/1.54533

[64] http://ssd.jpl.nasa.gov /?planet_eph_export [retrived October 27, 2011].

[65] E. M. Standish, "'JPL planetary and lunar ephemerides, DE405/LE405."'JPL IOM 312F 98 048, 1998.

[66] Vokrouhlicky, D.; Farinella, P.; Mignard, F.,*Solar radiation pressure perturbations for Earth satellites. 1: A complete theory including penumbra transitions*, Astronomy and Astrophysics (ISSN 0004-6361), vol. 280, no. 1, p. 295-312

[67] Lawden, D.F., *Optimal Trajectories for Space Navigation,* Butterworths, London, 1963, pp. 54–68.

[68] Hazelrigg, G.A., "Globally Optimal Impulsive Transfers via Green's Theorem," *Journal of Guidance, Control, and Dynamics*, Vol. 7, No. 4, 1984, pp. 462-470. doi: 10.2514/3.19879.

[69] Zimmer, S.; Ocampo, C.; Bishop, R.; , "Reducing Orbit Covariance for Continuous Thrust Spacecraft Transfers," Aerospace and Electronic Systems, IEEE Transactions on , vol.46, no.2, pp.771-791, April 2010 doi: 10.1109/TAES.2010.5461656

[70] Ross, I.M., and Qi, G., "Low-Thrust, High-Accuracy Trajectory Optimization," *Journal of Guidance, Control, and Dynamics*, Vol. 30, No. 4, 2007, pp. 921-933. doi: 10.2514/1.23181.

[71] Gao, Y., "Near-Optimal Very Low-Thrust Earth-Orbit Transfers and Guidance Schemes," *Journal of Guidance, Control, and Dynamics*, Vol. 30, No. 2, 2007, pp. 529-539. doi: 10.2514/1.24836.

[72] Yue, Y., and Yang, Y., "Indirect Optimization for Finite-Thrust Time-Optimal Orbital Maneuver," *Journal of Guidance, Control, and Dynamics*, Vol. 33, No. 2, 2010, pp. 628-634. doi: 10.2514/1.44885.

[73] Simeoni, F., Casalino, L., Zavoli, A., and Colasurdo, G., "Indirect Optimization of Satellite Deployment into a Highly Elliptic Orbit," International Journal of Aerospace Engineering, vol. 2012, Article ID 152683, 14 pages, 2012. doi:10.1155/2012/152683.

[74] Colasurdo, G., Pastrone, D., "Indirect Optimization Method for Impulsive Transfer," AIAA/AAS Astrodynamics Conference, Scottsdale, AZ August 1-3, 1994, pag. 558–563, ISBN: 156347090X. Paper AIAA 94-3762.

[75] Zavoli, A., Simeoni, F., Casalino, L., and Colasurdo, G., "Optimal Cooperative Deployment of a Two-Satellite Formation into a Highly Elliptic Orbit," 2011 AAS/AIAA Astrodynamics Specialist Conference, July 31 - August 4, 2011, Girdwood, Alaska. Paper AAS 11-641.

Giudizio sulla Tesi del dottorando Francesco SIMEONI – XXV ciclo

"Cooperative deployment of satellite formations into highly elliptic orbit"

Sommario della tesi

Il lavoro svolto durante il dottorato ha riguardato lo sviluppo di codici per l'ottimizzazione indiretta delle traiettorie di trasferimento di satelliti in orbite geocentriche con elevata eccentricità. Questa classe di orbite sta attraendo molto interesse, rappresentando un'economica alternativa a orbite in prossimità dei punti Lagrangiani.

La prima fase dello studio è stata dedicata alla definizione di un adeguato modello dinamico che tenesse in conto di tutte le perturbazioni rilevanti per il trasferimento; in particolare si sono considerate la non-sfericità della Terra (in questo studio fino all'ottava armonica, ma il modello può essere esteso ad armoniche maggiori), le perturbazioni gravitazionali di sole e luna e la pressione di radiazione solare. Un'adeguata formulazione del problema ha permesso l'applicazione della teoria del controllo ottimale al sistema di equazioni così ottenuto in modo relativamente semplice e "meccanico", senza le difficoltà che alcuni autori ritengono insite nell'applicazione di metodi indiretti quando il modello dinamico diventa complesso. La successione degli archi di spinta è influenzata dalle perturbazioni (in particolare dalla luna) e risente quindi della data di partenza; è stata sviluppata, ed è stata testata con successo, una strategia basata sulla graduale introduzione delle perturbazioni, per ottenere la convergenza alla soluzione ottimale in tempi molto ristretti (circa tre minuti nei casi più complicati) per qualunque data.

La seconda fase dello studio ha avuto il compito di confrontare le prestazioni di diverse strategie per il trasferimento dei satelliti nell'orbita richiesta. Il caso scelto come oggetto di studio è stato la missione Simbol-X, con il trasferimento di due satelliti in una stessa orbita ellittica con un vincolo sulla distanza relativa al passaggio all'apogeo. Si sono confrontati il trasferimento dei satelliti in modo separato, con la classica strategia chaser-target (in cui uno dei satelliti "insegue" l'altro) e con una strategia cooperativa, valutando il guadagno in termini di massa finale che la strategia cooperativa può fornire (in particolare evidenziando l'influenza che la spinta ha su di esso). L'analisi ha anche riguardato il rischio di collisione, e si è dimostrato che può sempre essere evitato con una scelta opportuna della geometria della formazione finale.

La parte finale dello studio ha visto puntare l'attenzione su strategie di trasferimento subottimali con direzione di spinta costante in ciascun arco propulso (che presentano grandi vantaggi in termini operativi) e sugli effetti che dispersioni di spinta (modulo e direzione) hanno per quanto riguarda errori nell'orbita raggiunta e nel vincolo di formazione. L'analisi condotta ha dimostrato la piccola penalità

Politecnico di Torino – DIMEAS - Dipartimento di Ingegneria Meccanica e Aerospaziale
Corso Duca degli Abruzzi, 24 – 10129 Torino Italia
tel: +39 011 0906819 (Coordinatore) - +39 011 0906805 (Segreteria) - fax: +39 011 090 6899
e-mail Coordinatore: fulvia.quagliotti@polito.it

associata ad una spinta in direzione fissa (pochi grammi di propellente rispetto alla soluzione ottimale), giustificandone così l'uso. Dispersioni di spinta anche contenute possono portare a grandi ed intollerabili errori (anche fino a centinaia di chilometri), in particolare sul vincolo di formazione finale; in quest'ottica si è definita un'efficace strategia di controllo closed-loop che consente di ridurre fortemente gli errori fino a valori accettabili.

Prodotti della ricerca e pubblicazioni

Nel corso dei tre anni di dottorato sono state prodotte diverse memorie ed articoli su riviste internazionali, sia riguardanti il filone principale del dottorato, sia relative ad attività collaterali, sempre nell'ambito dell'ottimizzazione di traiettorie. Una parte della ricerca è stata svolta dal candidato presso il JPL, Jet Propulsion Laboratory di Pasadena (USA) nell'ambito del progetto Bando Alta Formazione. In tale periodo l'attività è stata condotta sotto la supervisione del prof. Nathan Strange nell'ambito di orbite cicliche tra Terra e Marte e ricerca di asteroidi atti a fornire materiali per la protezione di astronauti dalle radiazioni cosmiche.

Giudizio del Collegio

La tesi presenta l'applicazione di metodi di ottimizzazione indiretti ad un complesso problema di trasferimento orbitale di satelliti in formazione; l'uso di questi metodi, più veloci ed economici dal punto di vista computazionale dei metodi diretti usati tradizionalmente, rappresenta una novità per problemi di questo tipo (con modello dinamico complicato e vincoli di formazione e collision avoidance), e si è dimostrato estremamente efficace, grazie alle particolari strategie adottate dal candidato per garantire la convergenza alla soluzione ottimale; l'aver testato in modo esaustivo i codici sviluppati su una missione reale ha evidenziato l'utilità delle procedure proposte.

L'analisi ed il confronto tra le diverse strategie di trasferimento ha mostrato interessanti ed originali risultati, quali la stretta relazione tra livello di spinta, lunghezza degli archi propulsi e benefici derivanti da una strategia cooperativa rispetto all'approccio tradizionale chaser-target. L'analisi degli errori derivanti da dispersioni di spinta e la definizione di una strategia closed-loop per garantire il soddisfacimento dei vincoli di formazione rappresenta un ulteriore importante contributo fornito dal candidato.

In conclusione, sulla base dell'attività di ricerca svolta, si ritiene il dottorando Francesco Simeoni, pienamente meritevole di essere ammesso all'esame finale di Dottorato.

Il Coordinatore del Dottorato in Ingegneria Aerospaziale

Prof. Fulvia QUAGLIOTTI

Torino, 14/12/2012

Politecnico di Torino – DIMEAS - Dipartimento di Ingegneria Meccanica e Aerospaziale
Corso Duca degli Abruzzi, 24 – 10129 Torino Italia
tel: +39 011 0906819 (Coordinatore) - +39 011 0906805 (Segreteria) - fax: +39 011 090 6899
e-mail Coordinatore: fulvia.quagliotti@polito.it